Rock Mechanics and Rock Engineering (2023) 56:5293–5313
https://doi.org/10.1007/s00603-023-03329-9

ORIGINAL PAPER

Modeling Brazilian Tensile Strength Tests on a Brittle Rock Using Deterministic, Semi-deterministic, and Voronoi Bonded Block Models

Carlos E. Contreras Inga[1] · Sankhaneel Sinha[1,2] · Gabriel Walton[1] · Elizabeth Holley[3]

Received: 23 February 2022 / Accepted: 2 April 2023 / Published online: 25 April 2023

Abstract

This study aims to numerically investigate how various common simplifications of grain structure representation in bonded block models affect simulations of rock mechanical behavior. Specimens of Wausau granite were characterized mechanically through Brazilian tensile strength tests for this work. The samples were also characterized petrographically using thin section microscopy, scanning electron microscopy-based automated mineralogy, and visual inspection. Four types of representations of the Wausau granite samples were developed, including 6 detailed manually developed deterministic models, 6 semi-deterministic models, and 120 randomly generated representations (Voronoi models). First, a calibrated set of micro-properties was determined using the deterministic representations to simulate the Brazilian tensile strength measurements. Next, the study examined the ability of different Voronoi tessellations to adequately represent the grain structure for the purposes of accurate tensile strength simulation. This was evaluated by comparing Voronoi model results to the deterministic grain structure model results and laboratory test results. The findings of the study show that the four types of models used in this study can all provide realistic representations of the mechanical behavior of rock. The study confirms that standard Voronoi approximations of grain structures can be reasonably used in lieu of less practical, manually developed representations of the grain structure. Specifically, Voronoi models can properly replicate the geometric heterogeneity within the grain structure, even though they simplify some of its geometric attributes.

Highlights

- Four types of models of granite specimens were generated, each type representing the specimen grain structure with a different degree of realism.
- Brazilian tensile strength simulation results obtained using deterministic, semi-deterministic, and two different Voronoi structures were compared.
- Validity of randomly generated Voronoi models to adequately approximate the geometric heterogeneity within the grain structure was investigated.
- Voronoi models provided strengths nearly equivalent to those obtained from the more complex deterministic and semi-deterministic models.

Keywords Grain structure representation · Heterogeneity · Micro-properties · Bonded block models · Voronoi tessellations

✉ Carlos E. Contreras Inga
ccontreras@mines.edu; carlose.contreras@outlook.com

[1] Department of Geology and Geological Engineering, Colorado School of Mines, 1516 Illinois St., Golden, CO, USA

[2] WSP Golder, 426 N 44th St., Suite 375, Phoenix, AZ, USA

[3] Department of Mining Engineering, Colorado School of Mines, 1600 Illinois St., Golden, CO, USA

1 Introduction

Laboratory tests such as uniaxial compression, triaxial compression, and tensile strength tests are commonly used to characterize the strength of rocks. However, accurate characterization of the fracturing behavior of a rock can sometimes be difficult to achieve by these means due to the heterogeneous nature of the rock's grain structure. According to

experimental studies (Martin 1993; Eberhardt 1998; Staub et al. 2004), individual specimens of the same rock type can present variations in fracturing behavior and associated strength because of grain-scale heterogeneities. The heterogeneities of the rock grain structure cause complex micromechanical interactions and generate localized tensile stress concentrations that result in fracture development within a rock undergoing compressive loading (Diederichs 2003; Gao et al. 2016; Liu et al. 2018; Wang and Cai 2018). Heterogeneity can present due to elastic mismatch between constituent mineral grains, difference in grain shape and size, and/or presence of micro-flaws, such as pores, cleavage, and strings of grain boundary cavities (Sprunt and Brace 1974; Tapponnier and Brace 1976; Dey and Wang 1981; Kranz 1983; Cunha 1990). Thus, the grain structure heterogeneity controls the emergent macroscopic mechanical response of the intact rock (Lan et al. 2010; Mahabadi 2012; Gao et al. 2016). Lan et al. (2010) formally classified the sources of heterogeneity in intact rocks into three groups: (i) geometric heterogeneity related to variability in size and shape of the mineral grains, (ii) deformability heterogeneity associated with the contrasts among mineral grains in terms of density and elastic properties, and (iii) contact heterogeneity linked to the variability of the stiffness, length, orientation, and distribution of contacts between mineral grains. Numerous experimental studies (Olsson 1974; Singh 1988; Fredrich et al. 1990; Shea and Kronenberg 1993; Wong et al. 1996; Eberhardt et al. 1999; Tuğrul and Zarif 1999; Přikryl 2001; Güneş Yilmaz et al. 2011; Keikha and Keykha 2013; Yesiloglu-Gultekin et al. 2013; Sajid et al. 2016; Cowie and Walton 2018) have explored the effects of grain size and mineral content variability on the mechanical response of rock under loading, but these studies do not provide a clear consensus on the influences of specific grain structure attributes.

In recent decades, numerical modeling has been increasingly used to quantitatively investigate damage processes of brittle rocks. Notably, numerical modeling allows one to simulate conditions that are difficult to attain and study in the laboratory (Li et al. 2017a, 2019). Numerical modeling approaches for simulation of brittle rock damage are usually classified into three categories: (i) continuum, (ii) discontinuum, and (iii) hybrid continuum–discontinuum (Jing 2003; Potyondy and Cundall 2004). The continuum approach represents the rock as a single continuous body and employs constitutive relations and associated failure criteria to define rock damage (Jing 2003), but it is unable to explicitly represent fracture development. The common continuum modeling approaches are Finite Element Method (FEM) and Finite Difference Method (FDM) (Jing 2003). In contrast, discontinuum and hybrid continuum–discontinuum approaches explicitly simulate rock damage development under various loading conditions without using pre-defined macroscopic constitutive models (Lisjak and Grasselli 2014; Zhang and Wong 2018; Wang and Cai 2019). Detailed descriptions of these approaches can be found in the literature (Jing and Hudson 2002; Jing 2003; Jing and Stephansson 2007; Bobet et al. 2009) and are beyond the scope of the current study.

Discontinuum and hybrid methods can represent the heterogeneity within crystalline rocks more accurately than continuum methods (Zhang and Wong 2018). The Discrete Element Method (DEM) and the Finite Discrete Element Method (FDEM) are the most commonly applied approaches for rock damage modeling among the discontinuum and hybrid methods, respectively. The DEM simulates rocks as assemblies of discrete particles or blocks, which interact between each other and separate as fractures develop (Cundall 1971; Jing and Hudson 2002; Jing and Stephansson 2007; Lisjak and Grasselli 2014). The hybrid FDEM, can represent grains of irregular shape by connecting several triangular elements (Munjiza 2004) starting from a continuum representation of the rock that progressively develops new fractures and separates into discrete bodies (Lisjak and Grasselli 2014). Among DEM models, the Bonded Particle Model (BPM) and Bonded Block Model (BBM) approaches are commonly used for simulating intact rock behavior. BPMs represent grains as circular or spherical particles bonded at their contacts (Cundall and Strack 1979; Potyondy and Cundall 2004; Bewick et al. 2014). Since its introduction, a number of limitations were identified in BPM (Cho et al. 2007) and modifications were proposed to overcome these limitations (Potyondy and Cundall 2004; Cho et al. 2007; Potyondy 2012; Scholtés and Donzé 2013; Ding and Zhang 2014). Many of these modifications attempted to overcome the lack of particle–particle interlocking in BPM by fusing neighboring spheres/discs. BBMs, on the other hand, represent grain structures as collections of polygonal or polyhedral blocks (or grains) bonded at their interfaces (or grain–grain contacts) (Garza-Cruz et al. 2014).

The Voronoi tessellation approach is usually applied to generate the grain structure for a BBM, since the mathematical process of Voronoi tessellation is the most convenient technique to randomly generate polygonal or polyhedral shapes. Polygonal blocks with four or more sides (or complex polyhedral blocks in 3D) generated with Voronoi tessellations are usually referred to as Voronoi blocks (Ghazvinian et al. 2014; Li et al. 2019; Sinha and Walton 2020). Triangular blocks (or tetrahedral blocks in 3D) produced with a modification of the Voronoi logic are called trigons (Gao and Stead 2014). The Grain-Based Model (GBM) approach was introduced in BPMs to improve the representation of grain structures by adding grain-boundaries defined by smooth joint elements to a BPM, which are often defined using Voronoi tessellations (Bahrani et al. 2014). Similarly, the hybrid FDEM uses the GBM approach to define the grain structure through Voronoi

tessellations (Abdelaziz et al. 2018; Li et al. 2021a). More details about all these methods can be found in the literature (Munjiza 2004; Bahrani et al. 2014; Ghazvinian et al. 2014; Lisjak and Grasselli 2014; Abdelaziz et al. 2018; Zhang and Wong 2018).

It is generally recognized that assemblies of Voronoi polygonal/polyhedral blocks provide more realistic representations of grain structure geometric heterogeneity as compared to assemblies of other block shapes (Ghazvinian et al. 2014; Gao et al. 2016; Wang and Cai 2018, 2019; Li et al. 2019). This is because they provide more realistic grain interlocking within the grain structure. Voronoi tessellations have been widely used to simulate grain structures for this reason (Ghazvinian et al. 2014; Abdelaziz et al. 2018; Sinha and Walton 2018, 2020; Wang and Cai 2018, 2019). Several studies have numerically examined the influence of grain structure heterogeneity on the mechanical behavior of rock using Voronoi tessellations. Most of these studies have focused on the effects of average grain size and grain size distribution (Kazerani and Zhao 2010; Ghazvinian et al. 2014; Nicksiar and Martin 2014; Fabjan et al. 2015; Azocar 2016; Gao et al. 2016; Gui et al. 2016; Peng et al. 2017a, 2017b, 2021; Liu et al. 2018; Li et al. 2020, 2021a; Xu et al. 2020; Contreras Inga et al. 2021). Some studies have also attempted to incorporate true or 'deterministic' grain structures derived from scanning electron microscope or digital image processing techniques in grain-based models (Tan et al. 2016; Li et al. 2017b, 2019; Park et al. 2017), but the vast majority have employed stochastically generated block structures (e.g., Kazerani and Zhao 2010; Ghazvinian et al. 2014; Nicksiar and Martin 2014; Fabjan et al. 2015; Sinha et al. 2020). As pointed out by Wang and Cai (2018), BBMs with block structures that are statistically similar to the actual grain size distribution of the target rock unit are often computationally intensive and impractical for calibration. The effects of grain shape (Azocar 2016; Mayer and Stead 2017; Zhu et al. 2017; Xu et al. 2020; Contreras Inga et al. 2021; Li et al. 2021a), mineral arrangement (Lan et al. 2010; Fabjan et al. 2015; Gui et al. 2016; Liu et al. 2018; Zhou et al. 2019; Contreras Inga et al. 2021), micro-properties (i.e., properties of grains and grain–grain contacts within the model) (Sinha and Walton 2020; Contreras Inga et al. 2021), mineral composition (Nicksiar and Martin 2014; Li et al. 2021a), and fabric orientation (Ghazvinian et al. 2014) have also been investigated. Contreras Inga et al. (2021) investigated the influence of various aspects of grain structures generated using a Voronoi tessellation approach on rock unconfined compressive strength prediction using BBMs. It was observed that the stochastic effects introduced by the mineral arrangement represented in Voronoi models and the randomness of Voronoi grain structure generation have a significant influence on rock strength predictions, whereas average grain size and grain shape have a limited effect. On average, however, it was observed that Voronoi grain structure models could provide realistic rock strength predictions when used in combination with appropriate micro-properties (Contreras Inga et al. 2021).

Although it is well-established that Voronoi block assemblies can reasonably approximate grain interlocking in low porosity igneous rocks in contrast to assemblies of circular/spherical or triangular/tetrahedral grains, it has not yet been determined to what extent the simplifications inherent in the Voronoi approach affect mechanical behaviors compared to more detailed and realistic grain structure representations. To better understand the impact of grain structure simplifications sought in prior studies, multiple Brazilian Tensile Strength (BTS; International Society for Rock Mechanics 1978; Li and Wong 2013; Perras and Diederichs 2014; Li et al. 2021b) simulations were performed with BBM grain structures of differing degrees of complexity and a calibrated set of micro-properties. This approach differs from previous studies (e.g., Contreras Inga et al. 2021), which have considered variations in basic grain structure parameters (e.g., grain size and grain shape) without altering the overall level of complexity of the grain structure representation. The approach is novel in the sense that this is the first-time geometric heterogeneity is studied in the context of BBM by simplifying block structures that are derived deterministically from real specimens. The ability to systematically simplify the same deterministic block structure allowed for modifying grain shape, grain size distribution, and mineral arrangement. The outcomes from this study will assist future researchers in selecting a grain structure representation that is suitable to a particular problem.

There are three reasons for selecting the BTS test as the focus of this study: (1) specimen preparation and testing procedure is much simpler than the direct tensile strength test, although the stress state in a BTS test is similar to a confined direct tensile test (Diederichs 1999). In general, BTS yields a higher tensile strength in comparison with a direct tension test, and an empirical correction can be applied to estimate the direct tensile strength (Perras and Diederichs 2014). Since the BTS test was conducted in the laboratory and thereafter used directly as a calibration target in the BBM, the aforementioned difference in stress state and strength was not a point of concern in this study. (2) Given the high surface area to volume ratio of the specimens, it was possible to map the grain structure in a non-destructive manner by simply observing the ends of the specimen, (3) The BTS test has been successfully simulated by numerical modeling over the years and is a common calibration target in similar studies (Chen et al. 2004; Kazerani et al. 2012; Li and Wong 2013; Mahabadi et al. 2014; Dan and Konietzky 2014; Sinha et al. 2020). It is acknowledged here that continuum approaches (FEM/FDM) can also be used to model BTS tests, as has been demonstrated by Chen et al. (2004),

Yu et al. (2006), and Villeneuve et al. (2012), among others. However, continuum models are unable to explicitly simulate the separation of grain boundaries undergoing failure and do not capture the effect of elastic heterogeneity in its entirety (Zhang and Wong 2018). Our choice of modeling approach, i.e., BBM, is based on the aforementioned drawbacks of continuum models and is part of an ongoing effort by the authors to understand the capabilities and limitations of the BBM approach (Sinha 2020; West et al. 2020; Contreras Inga et al. 2021). The conclusions drawn might be equally applicable to other discontinuum and hybrid modeling techniques, but further studies are required to confirm this by reproducing the results shown here (or similar).

This study utilizes different types of representations of the grain structure of the Wausau granite to examine the effect of the grain structure representation on the capabilities of BBMs for the simulation of the mechanical behavior of brittle rock. Four types of models (deterministic, semi-deterministic, Voronoi with heterogeneous grain size, and Voronoi with uniform grain size) were generated and evaluated in the context of simulated and actual Brazilian tensile strength tests. The input micro-parameters were calibrated to match the laboratory test results using the deterministic grain structure model. Each type of model, therefore, represents the grain structure of the Wausau granite with a different degree of realism. Overall, this study directly evaluates the ability of randomly generated Voronoi models to approximate the geometric heterogeneity within the grain structure of intact rock.

2 Modeling the Wausau Granite Using Bonded Block Models

This study compares the results of different BBM models of Wausau granite in Brazilian strength test simulations to actual tests conducted in the laboratory. Since the study focuses on the influence of grain structure representation on BBM response, a single set of micro-properties was used for all simulations.

2.1 The Wausau Granite

Sims et al. (1993) describe the Wausau granite as a dark red medium- to coarse-grained alkali–feldspar granite mostly exposed in the central region of Wisconsin. The specimens used in this study were obtained from a quarry in the Marathon County, Wisconsin. Standard thin sections of the Wausau granite were prepared for petrographic analysis and Scanning Electron Microscopy (SEM)-based automated mineralogy. The automated mineralogy analyses were conducted at the automated mineralogy laboratory of the Department of Geology and Geological Engineering at the Colorado School of Mines using a TESCAN Integrated Mineral Analyzer (TIMA). The TIMA is based on a scanning electron microscope TESCAN–VEGA-3 model LMU VP-SEM and controlled by the TIMA3 software. The system relies on four energy dispersive X-ray (EDX) spectrometers for spectral data acquisition. Such spectrometers are set at a beam stepping interval of 15 μm, a beam intensity of 14, and an acceleration voltage of 24 keV. The system employs Monte Carlo simulations to model the interactions between the beam and the specimen. Acquired spectral data are compared to spectra kept in a look-up table to determine the mineral composition at each acquisition point. Results reported by the TIMA3 software are presented as a spreadsheet with the areal percentage mineral composition in the look-up table. The thin section petrography identified k-feldspar, plagioclase, quartz, and biotite as more abundant minerals in the specimens of Wausau granite. Figure 1 shows photos

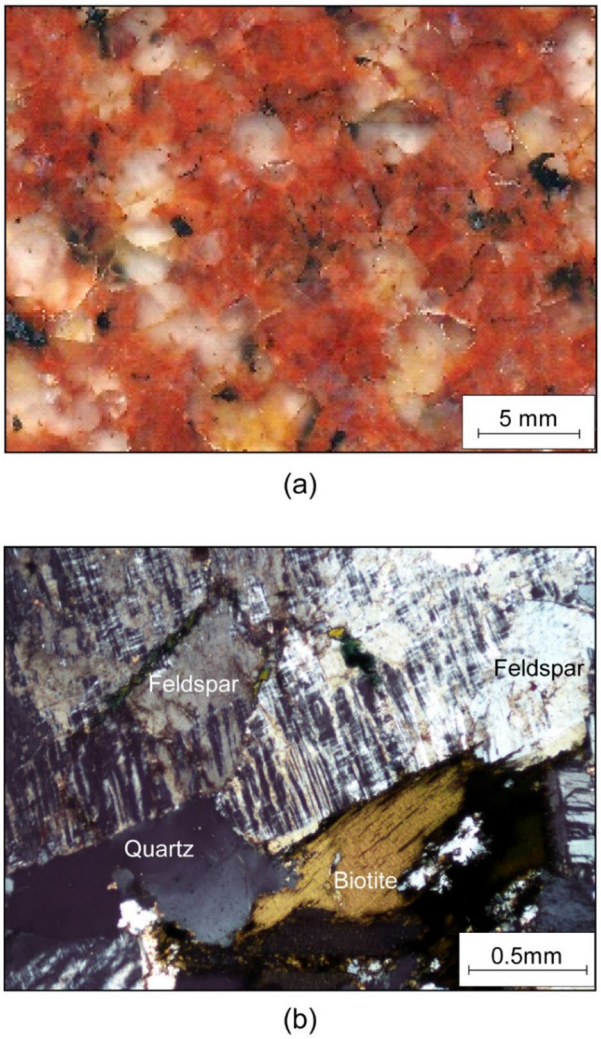

Fig. 1 **a** Hand specimen, and **b** Thin-section photomicrograph of the Wausau granite under cross-polarized light

of the Wausau granite in a hand specimen and a thin section. LaBerge and Myers (1983) and Sims et al. (1993) reported the presence of irregular intergrowth or exsolution of sodic and potassic feldspar in Wausau granite, and these textures were also identified in this study.

Three disk specimens employed for the Brazilian Tensile Strength (BTS) tests were characterized in terms of mineral composition and grain diameter. The mineralogical composition of each face of the disk specimens was examined through macroscopic petrographic characterization, and it was confirmed that the mineral composition varies on each one of the specimen faces, but all of them closely approximate the average composition obtained from automated mineralogy analyses. However, feldspar exsolutions within the Wausau granite samples made it difficult to determine the actual k-feldspar/plagioclase proportion accurately through macroscopic examination. Thus, for the purposes of this study, after defining visually the total feldspar content on each sample, the average k-feldspar/plagioclase proportion identified using automated mineralogy was used to estimate the sodic and potassic feldspar content of each disk specimen. The grain size was recorded in all the specimens in terms of the equivalent diameter of the grains (i.e., the area of each grain was converted to diameter based on a circular approximation using the equation: $Area = {}^{\pi}/_{4} diameter^2$). Similar to the mineral composition, the grain size distribution varies from specimen to specimen. The grain sizes by mineral were observed to be approximately log-normally distributed. The average overall apparent diameter varies from 1.0 mm to 1.3 mm among the samples. Table 1 summarizes the mineral composition per specimen, whereas Table 2 provides grain size mean (μ) and standard deviation (σ) parameters per specimen. The log-normal probability distribution is mathematically represented by (Papoulis and Pillai 2002)

$$f(x) = \frac{e^{-\left(\frac{(\ln x-\mu)^2}{2\sigma^2}\right)}}{x\sigma\sqrt{2\pi}} \tag{1}$$

Alternatively, grain size can be described using the classical particle-size distribution curve, and the corresponding D_{10}, D_{50}, and D_{90} values (equivalent diameters corresponding to 10%, 50%, and 90% finer, respectively) for each mineral type and for the whole face can be found in Table 3. The log-normal distribution parameters are more relevant to this study as they are direct input to the Voronoi generation software Neper (discussed in Sect. 2.2).

The Wausau granite was mechanically characterized using Uniaxial Compressive Strength (UCS; Contreras Inga et al. 2021) and Brazilian Tensile Strength (BTS) tests. The peak strength, crack damage stress (CD), crack initiation stress (CI), Young's modulus (E), and Poisson's ratio (ν) were identified from the UCS tests (Contreras Inga et al. 2021). The BTS was obtained from three tests (new to this study) conducted following ASTM International (2001) procedures in the Earth Mechanics Institute laboratory at Colorado School of Mines, which reached peak strengths of 11.5 MPa, 11.6 MPa, and 12.4 MPa. The disk-shaped specimens used in these tests were 51.4 mm in diameter, with a diameter-to-width ratio of 2:1. More details on these

Table 1 Mineral composition of Wausau granite

Specimen	Modal abundance (%)			
	Biotite	Quartz	Plagioclase	K-feldspar
Average (automated mineralogy)	3	32	41	24
BTS-1A	3	34	40	23
BTS-1B	2	39	37	22
BTS-2A	3	37	38	22
BTS-2B	3	30	42	25
BTS-3A	2	32	42	24
BTS-3B	3	34	39	24

Table 2 Grain size log-normal distribution parameters of Wausau granite

Specimen	Grain size (mm)									
	Biotite		Quartz		Plagioclase		K-feldspar		Overall	
	μ	σ	μ	σ	μ	σ	μ	σ	μ	σ
BTS-1A	0.7	0.4	2.3	1.3	1.1	0.6	1.2	0.6	1.2	0.7
BTS-1B	0.6	0.3	2.4	1.3	1.2	0.7	1.2	0.7	1.3	0.9
BTS-2A	0.6	0.3	2.2	1.2	1.1	0.6	1.0	0.5	1.1	0.7
BTS-2B	0.7	0.3	2.1	1.3	1.2	0.6	1.2	0.7	1.3	0.8
BTS-3A	0.5	0.3	2.0	1.1	1.0	0.5	1.0	0.5	1.0	0.6
BTS-3B	0.7	0.3	2.2	1.3	1.2	0.7	1.2	0.7	1.2	0.8

μ and σ are mean and standard deviation, respectively

tests can be found in Appendix A. Table 4 summarizes the mechanical properties obtained from the laboratory tests. The low Coefficient of Variation (CoV) values relative to other rocks and narrow confidence interval for the mean BTS (11.8 ± 0.56) based on the test results signify limited natural variability in Wausau granite, meaning that three tests reasonably characterize the indirect tensile strength of this rock (Langford and Diederichs 2015).

2.2 BBM Generation

The three disk-shaped specimens used in the BTS tests were used as the basis to generate different representations of the grain structure. Accordingly, four different groups of two-dimensional BBMs were generated for each one of the two faces of the disk specimens: deterministic, semi-deterministic, Voronoi with heterogenous grain size, and Voronoi with uniform grain size. Table 5 shows a comparison of the four types of models based on an assessment of the features of the true grain structure that they represent. All the BBMs were developed within 2D circular domains with the same diameter as the BTS specimens (i.e., 51.4 mm).

The first group of BBMs consists of deterministic representations of each one of the two faces of the three disk-shaped specimens, for a total of six deterministic models. Deterministic models are the closest approximation of the geometry of a grain structure. These models depict the size and shape of the grains and the actual mineral arrangement found within the laboratory specimens. Implementing these representations requires a manual characterization of the grain morphology and mineral arrangement within a rock specimen, which is highly time-consuming. To create the models, high-quality photographs of the faces of the specimens were digitized by manual creation of a series of

Table 3 Grain size distribution parameters of Wausau granite in mm

Specimen	Biotite			Quartz			Plagioclase			K-feldspar			Overall		
	D_{10}	D_{50}	D_{90}	D_{10}	D_{50}	D_{90}	D_{10}	D_{50}	D_{90}	D_{10}	D_{50}	D_{90}	D_{10}	D_{50}	D_{90}
BTS-1A	0.41	0.77	1.35	1.32	2.75	4.09	0.7	1.29	2.06	0.71	1.31	2.05	0.69	1.39	2.88
BTS-1B	0.41	0.67	1.33	1.43	2.74	4.35	0.73	1.35	2.13	0.7	1.49	2.3	0.74	1.56	2.96
BTS-2A	0.37	0.68	1.41	1.25	2.63	4.11	0.67	1.27	1.96	0.65	1.14	1.94	0.66	1.33	2.75
BTS-2B	0.39	0.74	1.41	1.13	2.73	4.07	0.74	1.42	2.19	0.78	1.37	2.2	0.74	1.47	2.75
BTS-3A	0.31	0.61	1.04	1.14	2.15	3.44	0.61	1.09	1.71	0.61	1.13	1.73	0.6	1.18	2.17
BTS-3B	0.4	0.72	1.28	1.29	2.55	3.42	0.69	1.35	2.26	0.66	1.42	2.19	0.67	1.48	2.73

D10, D50, and D90 are equivalent diameters corresponding to 10%, 50%, and 90% finer in a classical particle-size distribution curve

Table 4 Experimentally determined macro-mechanical properties of the Wausau granite

Property	Number of tests	μ	σ	CoV (σ/μ) in %
Density, ρ_m (kg/m^3)	11	2605	8	0.3
Uniaxial compressive strength, UCS (MPa)	11	226	21	9.3
Crack damage stress, CD (MPa)	11	220	19	8.6
Crack initiation stress, CI (MPa)	4	107	9	8.4
Young's modulus, E_m (GPa)	4	70	2	2.9
Poisson's ratio, ν_m	4	0.24	0.02	8.3
Brazilian tensile strength, BTS (MPa)	3	11.8	0.52	4.4

CoV is coefficient of variation

Table 5 Comparison of the representation complexity of the four types of BBMs

Type of BBM	Mineral composition	Average grain size	Grain size heterogeneity	Mineral arrangement	Grain shape
Deterministic	✓	✓	✓	✓	✓
Semi-deterministic	✓	✓	✓	✓	–
Voronoi with heterogeneous grain size	✓	✓	✓	–	–
Voronoi with uniform grain size	✓	✓	–	–	–

*✓ = properly represents this feature; – = not able to represent this feature

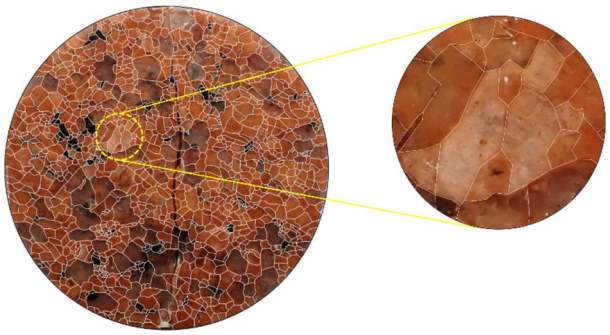

Fig. 2 Digitized surface of a BTS specimen prepared in CAD software; the white line segments shown were manually added to digitize the grain boundary shapes

straight-line segments in computer-aided design (CAD) software (Autodesk 2019). A length scale was assigned by setting the diameter of the photograph to the measured diameter of the specimens (i.e., 51.4 mm). Figure 2 shows an example of this digitization process. The grain outlines developed in the CAD software were later imported into UDEC to build the models. Concave and convex grains are represented in these models. Although these models are referred to as deterministic, some simplifications were adopted in their development. Specifically, these models only considered grains with an apparent diameter of 0.1 mm or greater and a minimum edge length of 0.05 mm. These simplifications were established to ensure consistency in the digitization process of the specimen faces and obtain models with comparable effective resolution. Once the grain structure was built in UDEC, the mineral type was assigned to the grains according to the spatial distribution observed in the actual specimens. Thus, each one of the six deterministic models has a unique mineral content proportion and mineral arrangement (see Table 2). The feldspar exsolutions present within the Wausau granite were modeled as grains of either pure k-feldspar or plagioclase. Accordingly, the distribution of k-feldspar and plagioclase grains was assigned randomly in each model. Considering that both types of feldspar present similar mechanical properties, variations in the k-feldspar/plagioclase proportion within the exsolutions are presumed to have a negligible effect on the rock macro-mechanical behavior.

The three other types of models (i.e., semi-deterministic, Voronoi with heterogeneous grain size, and Voronoi with uniform grain size) were generated as assemblies of 2D Voronoi tessellations, where each tessellation or cell represents a mineral grain. Mathematically, a Voronoi tessellation is the partition of an n-D space in an assembly of n-D polyhedral entities defined as zones of influence of a particular set of seeds, corresponding to their centers. The polyhedral entities fill the space within a domain without overlaps nor gaps (Quey et al. 2011). The resulting Voronoi grains are convex polyhedral cells, which intersect along planar faces and straight edges, and at vertices. The open-source software Neper (Quey 2019; Quey et al. 2011) was employed to generate the Voronoi grain assemblies. Neper uses Voronoi or Laguerre tessellations to generate polycrystal assemblies in 3D or 2D from a set of seeds positioned in space (Quey 2019). The main difference between Voronoi and Laguerre tessellations is that the latter is a generalization of Voronoi tessellations that allow for geometries that are not possible to achieve with Voronoi cells. This is possible using different weighted seeds that make boundaries between cells non-equidistant between seeds (Quey and Renversade 2018).

Six semi-deterministic models were generated for this study. Each semi-deterministic model is considered a simplification of a corresponding deterministic model, since not all features of the actual specimen grain structure are represented in the semi-deterministic version. The semi-deterministic grain structures were generated in Neper using the "centroiddiameq" option (Quey 2019). This option employs the centroid coordinates and equivalent diameter of each of the grains within the assembly, but it does not allow one to define the shape of the grains. The mineral arrangement and mineral composition of the actual granite specimens are properly represented in this type of model, given that such a grain structure representation uses the centroids of the grains and mineral arrangement in the deterministic models. In addition, using the grain diameters of the real specimens, the semi-deterministic models are able to accurately depict the grain size distribution of the specimen. However, this type of model cannot represent the actual shape of the grains, since the generated cells can only be convex polygons.

The third group of BBMs consists of 60 Voronoi models that properly represent the grain size heterogeneity within the Wausau specimens; 10 Voronoi models were stochastically generated per specimen face to properly account for the potential effects of randomness in the grain structure generation process on the simulated mechanical behavior. The morphological properties of the grains were defined in Neper using statistical distributions (i.e., mean, standard deviation, and distribution type) of grain size and shape. In Neper, the grain size is defined as the diameter (d) of a sphere of equivalent volume (or circle of equivalent area in 2D). The grain shape is defined using the sphericity (s) of the grain, which is the ratio between the area of a sphere of equivalent volume and the area of the grain (Quey and Renversade 2018). Sphericity is replaced by circularity in 2D, which is the ratio of the perimeter of a circle of equivalent area and the perimeter of the grain (Wadell 1933). Each model in a sub-group of 10 represents the same mineral content and grain size heterogeneity of the corresponding deterministic model, but a different set of randomly generated grains (specifically, 2 block structures were created per face with randomized mineral assignments). The grain size log-normal distribution

parameters identified from the actual specimen faces (see Table 2) were used to generate the grain structures in Neper. A 2D sphericity (i.e., circularity) equal to 0.88 was used in Neper to develop the models, as this value was qualitatively assessed to produce grain shapes that were approximately representative of the actual Wausau granite grains. The mineral types were randomly assigned to the grains within the models. The mineral content proportions (see Table 1) and grain size distributions per mineral type (see Table 2) were used as constraints. Specifically, 100% of the biotite grains have diameters between 0.0 and 2.0 mm; 16%, 68%, and 16% of the quartz grains correspond to ranges of 0.0–1.5 mm, 1.5–3.0 mm, and 3.0–6.0 mm, respectively; and 100% of the k-feldspar and plagioclase feldspar grains have diameters between 0.0 and 6.0 mm.

The last group of BBMs also consists of Voronoi models generated in Neper. As opposed to the previous group, the models within this group represent the grain size heterogeneity in the conventional way employed by previous studies (Chen et al. 2004; Chen and Konietzky 2014; Fabjan et al. 2015; Gui et al. 2016), with a grain size variability significantly lower than the observed variability in the real specimens. As in the previous case, six sub-groups of 10 models were built. The models within each sub-group represent the mineral content and average grain size measured in the Wausau granite specimens and depicted in the corresponding deterministic models. In Neper, the grain size distribution was denoted using the average/overall grain size measured in the granite specimens (see Table 2) and a uniform standard deviation of 0.25 mm for all models. A grain 2D-sphericity (i.e., circularity) value of 0.88 was applied in all the models. The mineral type was randomly assigned to the blocks within the grain structure using the mineral content proportions estimated in the granite specimens as the only constraint. Table 6 summarizes the geometric characteristics employed for the generation of the two different types of Voronoi models. Figure 3 shows the actual grain structure for one Wausau granite specimen face and its representations according to the approaches described above.

2.3 Constitutive Behavior of Intact Rock and Micro-Property Assignment

The software UDEC (Itasca Consulting Group Inc. 2014) was used to run the simulations presented in this study. UDEC allows for the simulation of grains within a BBM as rigid, elastic, or plastic blocks (Ghazvinian et al. 2014; Wang and Cai 2018; Zhang and Wong 2018). A constitutive relationship can be applied to the gains when they are modeled as elastic or plastic. The mechanical interactions along the common contact of two grains can be simulated through a joint constitutive model (Itasca Consulting Group Inc. 2014). In this study, the mineral grains were modeled as unbreakable elastic blocks with distinct density (ρ), Young's modulus (E), and Poisson's ratio (ν) for each mineral type. The use of elastic grains only allows failure to occur along the contacts between grains (Ghazvinian et al. 2014; Nicksiar and Martin 2014; Wang and Cai 2018). A similar simplification was applied in published studies that use BBMs (Kazerani and Zhao 2010; Lan et al. 2010; Chen and Konietzky 2014; Ghazvinian et al. 2014; Nicksiar and Martin 2014; Farahmand and Diederichs 2015; Chen et al. 2016). This simplification is appropriate for simulated behavior under unconfined or tensile loading

Table 6 Geometric characteristics of the 3D Bonded Block Models

Type of Voronoi model	Bonded block model	Grain diameter (mm)		Grain sphericity, s		Number of grains
		μ	σ	μ	σ	
Voronoi with grain heterogeneity	1-A	1.2	0.7	0.88	0.03	1361/1364
	1-B	1.3	0.8	0.88	0.03	1169/1159
	2-A	1.1	0.7	0.88	0.03	1475/1470
	2-B	1.3	0.7	0.88	0.03	1285/1289
	3-A	1.0	0.6	0.88	0.03	1952/1963
	3-B	1.2	0.7	0.88	0.03	1368/1379
Voronoi with uniform grain size	1-A	1.2	0.25	0.88	0.03	1366/1347
	1-B	1.3	0.25	0.88	0.03	1159/1165
	2-A	1.1	0.25	0.88	0.03	1479/1468
	2-B	1.3	0.25	0.88	0.03	1267/1276
	3-A	1.0	0.25	0.88	0.03	1939/1936
	3-B	1.2	0.25	0.88	0.03	1364/1358

The number of grains corresponds to the two grain structures built per face. For each of these grain structures, 5 realizations were generated by randomizing the mineral assignment (a total of $5 \times 2 = 10$ realizations per face)

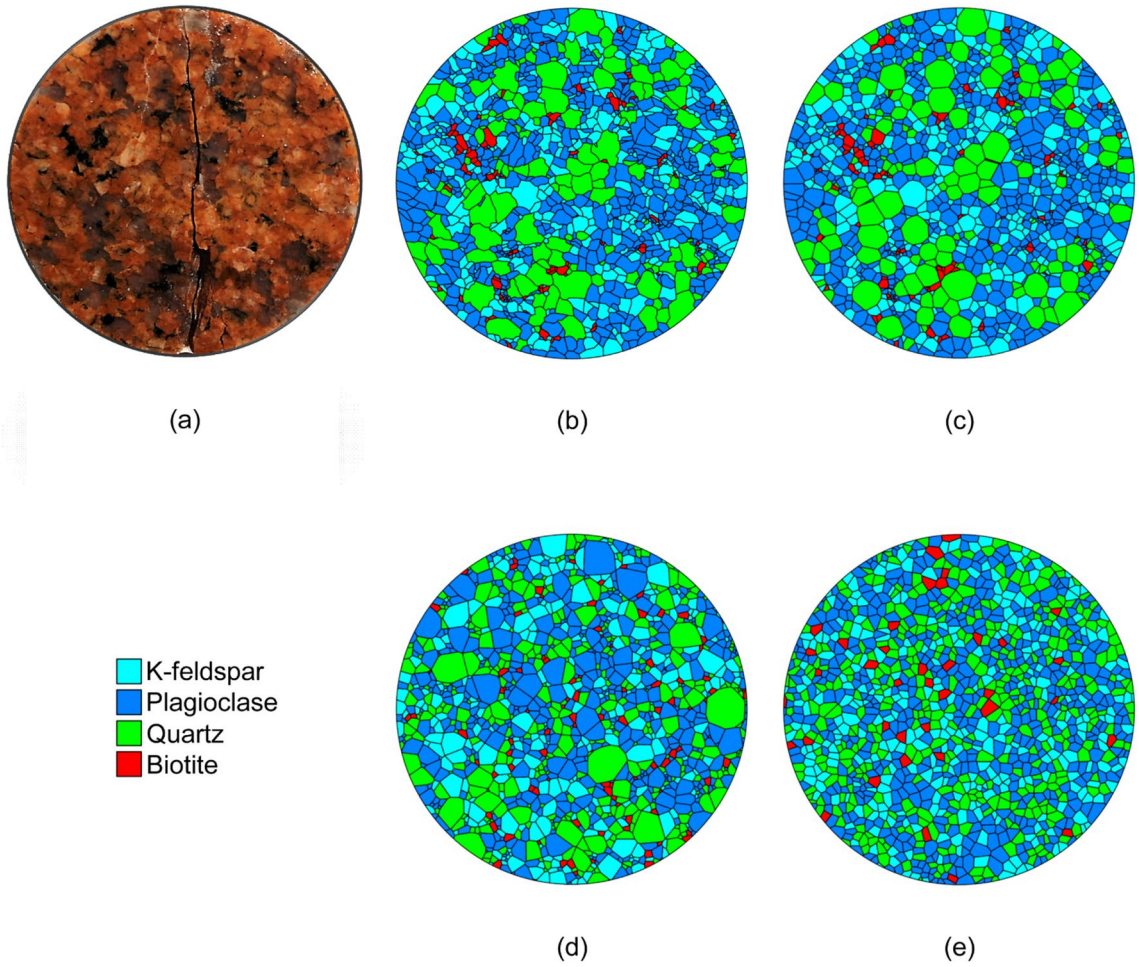

Fig. 3 **a** Disk-shaped specimen BTS-2, face B, of Wausau granite, and four corresponding representations: **b** deterministic, **c** semi-deterministic, **d** Voronoi with heterogeneous grain size, and **e** Voronoi with uniform grain size

conditions (Sinha and Walton 2020), as in this study. The grains were discretized into a mesh of deformable triangular finite-difference zones. Given the sensitivity of the simulation results to mesh size (Cai and Zhao 2000; Chen et al. 2000), a maximum triangular zone edge length of 0.8 mm was applied in all models to minimize the effect of mesh size. The resulting average grain edge length to zone edge length ratios are greater than or equal to 1.75, which agrees with the recommended ratio to achieve stable numerical results (Fabjan et al. 2015). A Coulomb slip-joint constitutive model with residual strength parameters was applied to the grain–grain contacts considering different attributes for each type of contact. Each contact was assigned a normal stiffness (k_n), shear stiffness (k_s), peak friction angle (φ), peak cohesion (C), peak tensile strength (σ_t), and residual friction angle (φ_r). The residual cohesion (C_r), and residual tensile strength (σ_{tr}) were assumed to be zero based on previous studies (Kazerani and Zhao 2010; Lan et al. 2010; Chen and Konietzky 2014; Gao and Stead 2014; Ghazvinian et al. 2014; Nicksiar and Martin 2014; Farahmand and Diederichs 2015; Chen et al. 2016). To calibrate the model, the micro-properties of Farahmand and Diederichs (2015) were used as a starting point, followed by systematically modifying the parameters until the simulated BTS for the deterministic BBM matched those measured in the laboratory. Tables 7 and 8 show the calibrated micro-properties used in this study.

Table 7 Grain micro-properties used by Farahmand and Diederichs (2015) and applied in the present study

Mineral type	Young's modulus E (GPa)	Poisson's ratio ν	Density ρ (g/cc)
K-feldspar	96.8	0.28	2.56
Plagioclase	88.1	0.26	2.63
Quartz	94.5	0.08	2.65
Biotite	33.8	0.36	3.05

Table 8 Contact micro-properties calibrated in the present study

Contact type	k_n (GPa/m)	k_s/k_n	C (MPa)	φ, $φ_r$ (°)	$σ_t$ (MPa)
KF/KF	2.3E+5	0.65	110.0	62.0, 5.0	22.8
KF/PL	2.1E+5	0.65	108.0	61.0, 5.0	20.8
KF/QZ	2.7E+5	0.65	76.0	53.0, 5.0	18.3
KF/BT	2.3E+5	0.65	60.0	48.0, 5.0	7.4
PL/PL	2.5E+5	0.65	112.0	63.0, 5.0	24.0
PL/QZ	2.3E+5	0.65	80.0	49.0, 5.0	18.3
PL/BT	2.3E+5	0.65	54.0	45.0, 5.0	14.6
QZ/QZ	2.8E+5	0.65	130.0	65.0, 5.0	22.8
QZ/BT	2.3E+5	0.65	57.0	52.0, 5.0	15.2
BT/BT	1.3E+5	0.65	88.0	55.0, 5.0	16.4

2.4 Numerical Test Setup

For the BTS test simulations, compressive loading was applied to the disk-shaped specimens through two rigid platens (Fig. 4). A constant vertical velocity was applied on both platens (top and bottom) to produce an effective loading velocity, v (i.e., − v/2 and v/2 applied to the top and bottom platens, respectively). The loading velocity and the damping mode strongly influence the simulation results (Sinha et al. 2022). Thus, to reach realistic simulation results, the loading velocity must be sufficiently slow enough given the damping conditions that are enforced to ensure that the model remains in a quasi-static equilibrium condition (Kazerani and Zhao 2010; Mayer and Stead 2017). Through a sensitivity analysis, a constant rate of 0.05 m/s was identified as a loading velocity below which changes in velocity had a negligible (i.e., < 4%) influence on the modeled strength. Since UDEC automatically calculates a timestep of approximately 10^{-8} s, the 0.05 m/s loading rate can be interpreted as approximately $5*10^{-6}$ mm/step. The damping mode for the simulations was set to "local" with a default damping coefficient of 0.8 (Itasca Consulting Group Inc., 2014). This form of velocity-proportional damping minimizes the effect of dynamic oscillations that could arise, while failure occurs within the model (Kazerani et al. 2012; Gao et al. 2016).

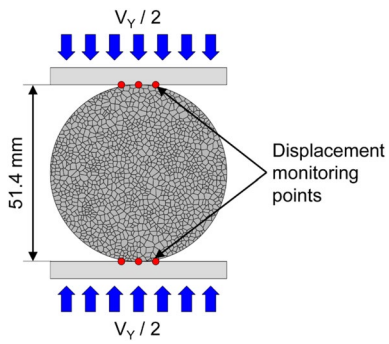

Fig. 4 Loading conditions and displacement tracking points for BTS test simulations

Axial displacements were obtained by averaging the displacements between three pairs of grid points located on the surface of the loading platens using a FISH script (Itasca Consulting Group Inc. 2014). The tensile stress was calculated from the total reaction forces measured on the surfaces of the platens using the standard BTS ($σ_t$) equation (International Society for Rock Mechanics 1978):

$$\sigma_t = \frac{2P}{\pi D t} \tag{2}$$

where P is the load at failure, D is the diameter of the specimen, and t is the thickness of the specimen. In addition, the development of tensile and shear fractures was tracked using a FISH script.

3 BTS Simulation Results and Discussion

3.1 Simulation Using Deterministic and Semi-deterministic Grain Structure Representations

Figure 5 and Table 9 present the results of the deterministic and semi-deterministic BTS test simulations for the six 2D grain structures modeled in this study (i.e., grain structures developed for each of the two faces of three disk specimens). The results indicate that compared to a target BTS value (i.e., BTS obtained in a laboratory test), both types of models approximate the actual test values with varying degrees of accuracy. The strengths from

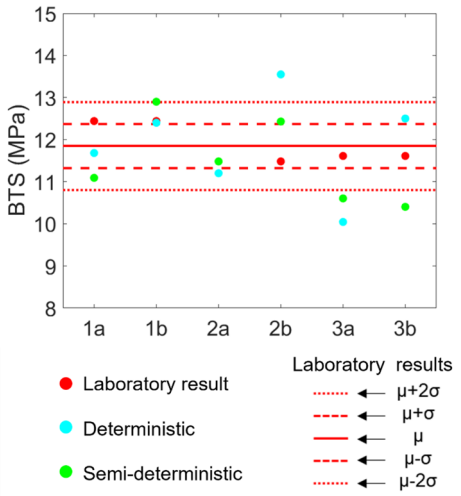

Fig. 5 Comparison of laboratory results (red dots) against corresponding deterministic (blue dots) and semi-deterministic (green dots) BTS per grain structure (i.e., grain structures described on each of the two faces of three disk specimens) (color figure online)

Table 9 Summary of simulated BTS with deterministic and semi-deterministic models

Grain structure	Laboratory	Deterministic		Semi-deterministic	
	(MPa)	(MPa)	Dif. [a] (%)	(MPa)	Dif. [a] (%)
BTS-1A	12.4	11.7	6	11.1	11
BTS-1B		12.4	0	12.9	− 4
BTS-2A	11.5	11.2	3	11.5	0
BTS-2B		13.5	− 18	12.4	− 8
BTS-3A	11.6	10	13	10.6	9
BTS-3B		12.5	− 8	10.4	10
Overall	11.8	11.8		11.5	

[a]Dif. = difference expressed as a percentage of the laboratory target value

deterministic models vary from 18% below to 13% above the target, whereas the strengths from semi-deterministic models fluctuate from 8% below to 11% above the target. In addition, the results indicate that both deterministic and semi-deterministic models were able to achieve approximate predictions of Wausau granite's BTS (i.e., within the range of variability estimated from laboratory tests), with the overall strength of the deterministic models matching the laboratory measurements. Although deterministic models closely replicate the grain structure geometry, 2 out of 6 strengths fall outside the BTS variability range registered in laboratory tests. Similarly, 2 out of 6 semi-deterministic models provided strengths outside the observed BTS variability range.

Figure 6 shows the stress–displacement curves and corresponding cumulative number of fractures (tensile and shear) obtained from the simulations with deterministic and semi-deterministic grain structures. The stress–displacement curves obtained from the BTS simulations using deterministic and semi-deterministic models (see Fig. 6) show similar pre-peak behavior in all cases. This similarity is more noticeable when comparing the curves obtained with a deterministic model and its corresponding semi-deterministic model; such pairs of curves closely match along the pre-peak section. Given that deterministic and semi-deterministic models have in common a detailed representation of the mineral arrangement and mineral size distribution, we can infer that both features have a strong effect on the pre-peak behavior of the rock. The simulations properly capture the exponential increase of the number of cracks, with a notably higher rate for the tensile cracks than the shear cracks as the simulation reaches the peak tensile strength.

3.2 Simulation Using Voronoi Grain Structure Representations

Voronoi models are not intended to be exact depictions of the mineral arrangement and grain geometry found in actual specimens of a rock. However, Voronoi models are expected to provide proper approximations of the grain structure

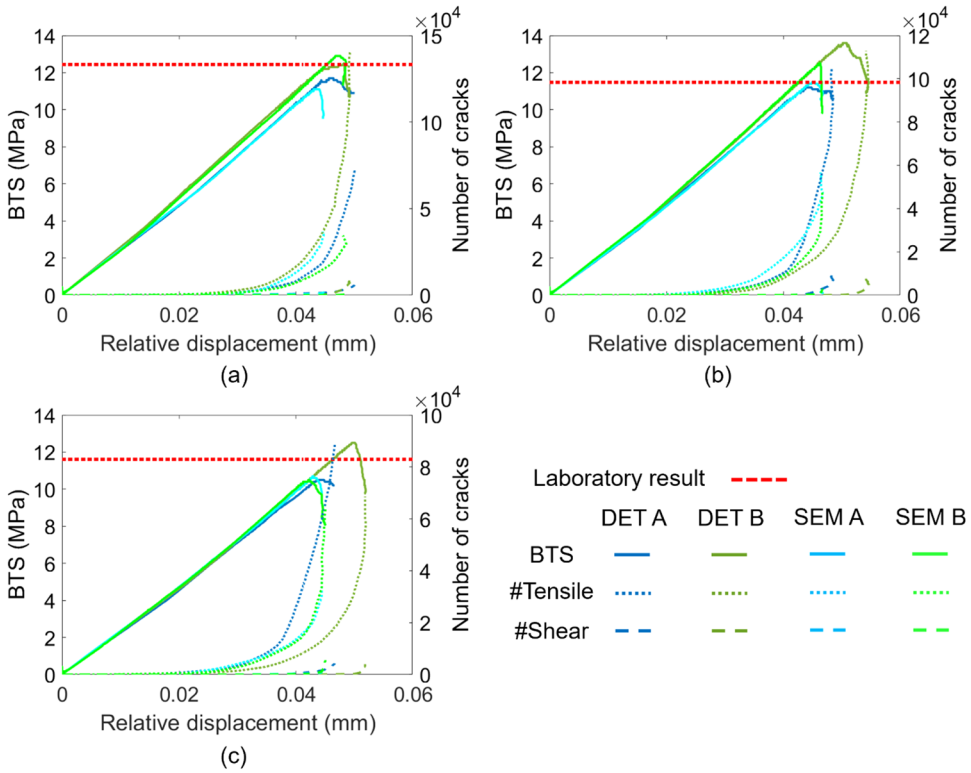

Fig. 6 Stress—displacement curves and cumulative number of tensile and shear cracks simulated using deterministic and semi-deterministic models of **a** specimen BTS-1, **b** specimen BTS-2, and **c** specimen BTS-3

heterogeneity. Given the stochastic nature of the Voronoi tessellation approach, multiple BBMs with equivalent grain structure heterogeneity can be generated. This portion of the study employs two types of Voronoi BBMs with different degrees of realism: (1) Voronoi models with heterogeneous grain size (hereafter referred to as Voronoi HGS), which represents the grain size variability for each mineral type; and (2) Voronoi models with uniform grain size (hereafter referred to as Voronoi UGS), which is the conventional Voronoi grain structure representation that only represents the rock's overall average grain size with limited variability. For the three specimens of Wausau granite used in this study, the respective experimental BTS values were compared against the deterministic and semi-deterministic results (i.e., mean predictions, obtained from two simulations in each case), as well as the Voronoi HGS and Voronoi UGS results (i.e., mean prediction and corresponding variability, based on 40 simulations in each case, twenty per face). Figure 7 shows such a comparison of BTS predictions made with the different models against laboratory test results. Figure 8 shows the final cracking state obtained with the four types of models presented in this study. All types of models are able to reproduce the typical failure pattern (i.e., dominated by tension cracks) obtained in laboratory BTS tests.

In the three cases corresponding to the three different laboratory specimens (see Fig. 7a–c), the stochastically generated grain structures represented in Voronoi HGS and Voronoi UGS models yield a variety of BTS values. This is expected, as each of the Voronoi grain structures is unique, and the grain structure is known to have a significant effect on the macroscopic response of BBMs (Ghazvinian et al. 2014; Fabjan et al. 2015; Azocar 2016; Insana et al. 2016). Voronoi HGS models provide average BTS 4–5% lower than the average experimental BTS (see Table 10) and an overall variability greater than the experimental variability (see Table 11). The average BTS with Voronoi HGS models falls within the Wausau granite's BTS variability range, as observed in laboratory tests. Similarly, Voronoi UGS models result in average BTS 2–4% higher than the actual BTS (see Table 10) and an overall variability greater than the experimental variability (see Table 11). The average BTS with Voronoi UGS models falls within the experimentally observed variability range. In addition, the average strength based on Voronoi UGS models is ~ 1 MPa higher than the

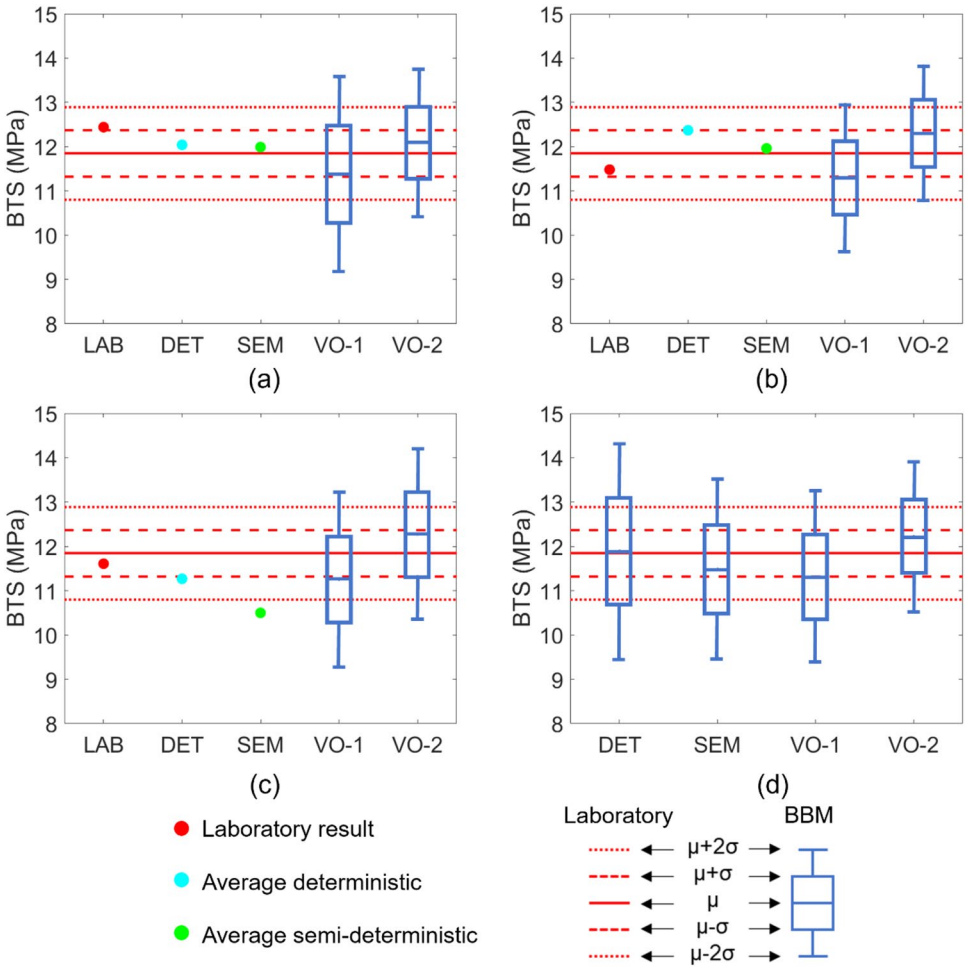

Fig. 7 Comparison of laboratory results (LAB) against corresponding deterministic (DET), semi-deterministic (SEM), Voronoi HGS (VO-1), and Voronoi UGS (VO-2) BTS. **a** comparison for specimen 1, **b** comparison for specimen 2, **c** comparison for specimen 3, and **d** overall comparison

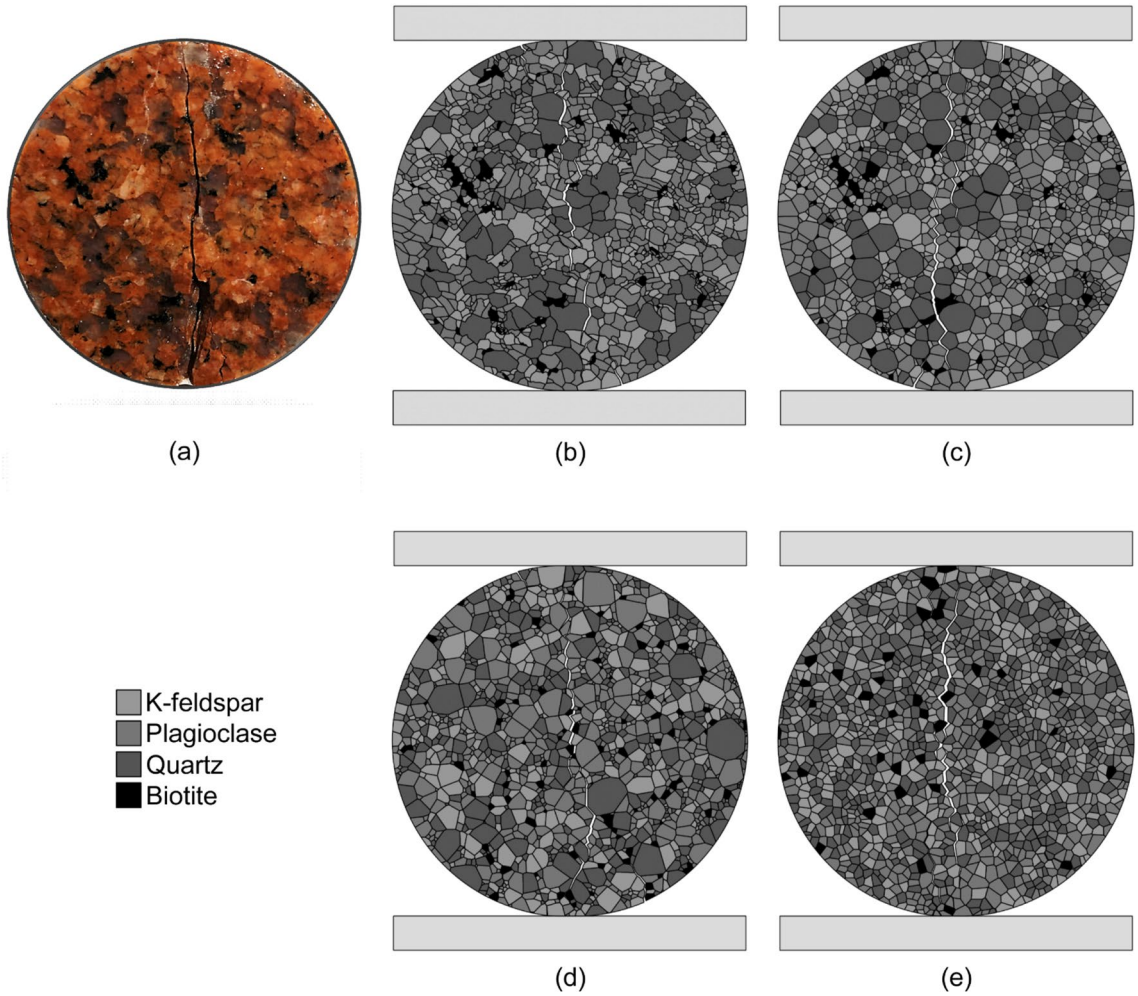

Fig. 8 **a** Fracture pattern observed in specimen BTS-2, face B, compared to the patterns obtained with the four corresponding types of models: **b** deterministic, **c** semi-deterministic, **d** Voronoi with heterogeneous grain size, and **e** Voronoi with uniform grain size

Table 10 Summary of the average BTS generated using each type of model

Grain structure	Laboratory	Deterministic		Semi-deterministic		Voronoi HGS		Voronoi UGS	
	μ (MPa)	μ (MPa)	Dif. [a] (%)	μ (MPa)	Dif. [a] (%)	μ (MPa)	Dif. [a] (%)	μ (MPa)	Dif. [a] (%)
Specimen 1	11.8	n/a	n/a	n/a	n/a	11.4	− 4	12.1	2.1
Specimen 2		n/a	n/a	n/a	n/a	11.3	− 4.7	12.3	3.8
Specimen 3		n/a	n/a	n/a	n/a	11.3	− 5	12.3	3.6
Overall simulations		11.9	0.4	11.5	− 3	11.3	− 4.6	12.2	3.2

[a]Dif. = difference expressed as a percentage of the laboratory mean value

Table 11 Summary of the overall standard deviations generated by each type of model. CI is confidence interval (Sheskin 2003)

Grain structure	Laboratory		Deterministic		Semi-deterministic		Voronoi HGS		Voronoi UGS	
	σ (MPa)	95% CI	σ (MPa)	95% CI	σ (MPa)	95% CI	σ (MPa)	95% CI	σ (MPa)	95% CI
Overall simulations	0.5	[0.3, 3.3]	1.2	[0.8, 3.0]	1.0	[0.6, 2.5]	1.0	[0.8, 1.2]	0.8	[0.7, 1.0]

average strength from the Voronoi HGS models. This behavior is consistent with the findings of Peng et al. (2017a, b) and Xu et al. (2020), who examined the effect of grain size heterogeneity and identified that as grain size heterogeneity increases, the rock strength decreases.

Figure 7a–c also shows that the average strengths resulting from deterministic and semi-deterministic models fall within the variability range obtained from Voronoi HGS and Voronoi UGS models. This indicates that Voronoi representations are able to capture the grain structure heterogeneity depicted in detailed models (i.e., deterministic and semi-deterministic models). In addition, the similarities of the distributions of BTS for specimens 1, 2, and 3 (using Voronoi HGS and Voronoi UGS models) indicate that variations in average mineral content (see Table 2) and average grain size (see Table 4) of the rock have a limited effect on the model behaviors.

Figure 7d summarizes the overall distributions for the four types of models developed in this study (i.e., all models for all specimens and faces). Such distributions present similar average strengths (11.3–12.2 MPa) and limited variability in strength standard deviations (0.8–1.2 MPa). Given that the same set of micro-properties was applied in the simulations with the four types of models, the similarities between the strength distributions suggest that even the simplest Voronoi representations appropriately represent the geometrical heterogeneity within the Wausau granite's grain structure that is relevant to tensile strength as effectively as the more detailed representations (i.e., deterministic, and semi-deterministic representations). Nevertheless, as identified previously (see Fig. 7a–c), the average BTS obtained with Voronoi HGS tend to be lower than the average obtained with Voronoi UGS. As the Voronoi HGS models are closer to the detailed models in terms of realism than the Voronoi UGS models are, it was originally expected that Voronoi HGS models would provide strength estimates that closely match those obtained with detailed models. However, Fig. 7d shows that the average BTS obtained with Voronoi UGS models is closer to the average BTS provided by the detailed models. This result could indicate that Voronoi UGS models provide a more realistic approximation of the degree of interlocking within the grain structure. The distributions provided by deterministic and semi-deterministic models may not provide conclusive evidence to confirm this presumption, since a small number of cases (six) were considered. Figure 7d also shows how the experimental variability range of the Wausau granite compares to the distributions for the four types of models. The distributions obtained with the four types of models have higher and lower average strength (− 5% to 3% higher) and higher standard deviation than the experimental BTS distribution. In addition, the UGS, HGS, and semi-deterministic models exhibit lower apparent variability than the deterministic models, but the difference is not statistically significant (refer to the 95% confidence intervals in Table 11). As mentioned previously, the similarities between the distributions suggest that the four types of models considered all reasonably represent the heterogeneity of the grain structure of Wausau granite for the purposes of tensile strength simulation.

Finally, to ensure that the effect of grain structure/geometric heterogeneity is not substantially dependent on the choice of micro-properties or material heterogeneity, two tasks were undertaken: (1) a sensitivity analysis on the contact tensile strength, and (2) running models with homogenized (i.e., single parameter set) grain (Table 7) and contact properties (Table 8). The approach and associated results can be found in Appendix B. Although some interesting trends were observed, the results are generally consistent with those presented here.

3.3 Discussion on Model Results

Prior studies (e.g., Nicksiar and Martin 2014; Fabjan et al. 2015; Mayer and Stead 2017; Xu et al. 2020; Contreras Inga et al. 2021) evaluated the ability of Voronoi models to realistically represent grain structure heterogeneity by varying individual parameters, such as grain size and grain shape. However, the degree to which the simplifications intrinsic in the Voronoi approach affect the accuracy of mechanical behavior predictions has not been evaluated in the literature. In contrast to previous work, this study presented models of the same specimens with different degrees of grain structure realism. These models allowed us to examine to what extent results obtained with Voronoi representations differ from results obtained using more detailed and realistic depictions of grain structure.

Many of the model results presented in this study show noticeable differences compared to the laboratory results. In general terms, once the constraints that control a given numerical simulation are properly defined, the ability to realistically simulate the mechanical behavior of rocks depends on the representation of the grain structure and the micro-properties applied in a BBM. With that said, we hypothesize several potential explanations for the observed differences between the laboratory and model results.

Using 2D models to represent the grain-structure can have a significant effect on the validity of the results, as the 2D representations are simplifications of 3D grain structures. For Wausau granite, the 2D geometrical information obtained by digitizing the faces of the BTS specimens cannot be directly converted to a unique 3D structure, because the grain size is smaller than the thickness of the specimens. Therefore, even in the case of deterministic and semi-deterministic models, the 2D grain-structure representations developed using individual faces are imperfect depictions of the complete 3D grain-structure of the laboratory

specimens. Accordingly, we acknowledge that even if a 2D grain-structure representation is highly accurate (e.g., deterministic representation), the 3D mechanical interactions between grains are not completely captured in a 2D representation. In addition, there are multiple possible 2D representations for the same 3D grain-structure (i.e., generated from diametrical sections, in the case of a disk-shaped specimen). Each one of these possible 2D simplifications has a unique mineral arrangement and grain geometric heterogeneity that could lead to different predictions of mechanical behavior. This is evident from a comparison of the model strengths for the two faces of the deterministic specimens (Table 9), where the degree of variation can be considered a rough proxy for potential magnitude of the effect of 2D simplification. In any case, the four types of 2D models used in this study produced similar average strengths with limited variability. This suggests that the heterogeneity of the grain structure geometry is adequately represented in each of the 2D Voronoi models with unique grain structure configurations. For practical reasons, conventional Voronoi models are recommended over the more detailed alternatives (i.e., deterministic and semi-deterministic models). In contrast to more detailed models, multiple randomly generated Voronoi models can be easily and rapidly generated to evaluate the range in modeling results depending on stochastic aspects of the grain structure representation.

In addition, other simplifications applied in the models may have a greater effect than was originally expected. For example, modeling the grains as unbreakable blocks may limit the representation of fracture propagation within the grain structure, as the development of transgranular fractures is not represented in the simulations. Although intergranular fracturing is expected to be the dominant process, in reality, some non-zero number of transgranular fractures do occur before the peak tensile strength is reached. Modeling only intergranular fracturing potentially leads to overestimations of the peak tensile strength due to the enhanced interlocking among grains.

Realistic predictions may not be obtained if the heterogeneity of grain and contact properties (i.e., micro-properties) is not adequately represented in the model, even when the geometric heterogeneity within the grain structure is properly depicted. The representation of property heterogeneity is achieved in this study by assigning different sets of micro-properties to each mineral type. However, property heterogeneity within a single mineral type is not considered in the models. This simplification of property heterogeneity could potentially lead to an unrealistic model response. Besides the above, as some of the micro-properties used in the simulations are based on calibration to Lac du Bonnet granite properties (Farahmand and Diederichs 2015), they are not a perfect representation of the corresponding micro-parameters for Wausau granite, either for physical reasons (e.g., the actual properties of the same minerals varied slightly between the two rocks) or numerical reasons. It is, therefore, uncertain to what degree these properties can be universally applied to the same mineral grains and grain-to-grain contact types in other rocks.

4 Conclusions

This study examined the capabilities of four different types of grain structure representations with different degrees of realism for the simulation of brittle rock tensile strength. The grain structure representations were implemented in Bonded Block Models (BBMs) using a calibrated set of micro-properties. Detailed 2D representations of the grain structure (i.e., deterministic and semi-deterministic models) provided realistic estimates of the BTS of Wausau granite. These models closely approximated the mineral content, mineral arrangement, grain size heterogeneity, and grain shape heterogeneity (the shape only in the deterministic models) observed in tested specimens.

Voronoi models were confirmed to provide strength estimates following distributions nearly equivalent to those obtained using the more detailed models. This indicates that Voronoi models are as effective as models using more sophisticated grain structure representations in simulation of rock tensile fracturing behavior. In addition, this suggests that Voronoi models properly approximate the geometric heterogeneity of the grain structure, even without including many details of the grain structure geometry. We believe this is a highly significant outcome, since it effectively validates the simplified modeling approaches that have been used by the scientific community and practitioners to date. Accordingly, a Voronoi grain structure representation that properly captures the mineral content proportions and the overall average grain size can be considered an appropriate approximation of reality, at least in the context of tensile damage processes.

Appendix A: Brazilian Tensile Tests

Three BTS tests on Wausau Granite were conducted following the ASTM International D3967-95a (2001) procedures in the Earth Mechanics Institute laboratory at the Colorado School of Mines. The specimens were loaded at 110 N/sec until failure occurred via formation of diametral/axial fractures. Figure 9 shows the three specimens before and after completion of the tests. The specimen geometrical details are as follows: (1) BTS-1—diameter = 51.4 mm, thickness = 25.1 mm; (2) BTS-2—diameter = 51.4 mm, thickness = 25.2 mm; (2) BTS-3—diameter = 51.4 mm, thickness = 24.7 mm. The load recorded

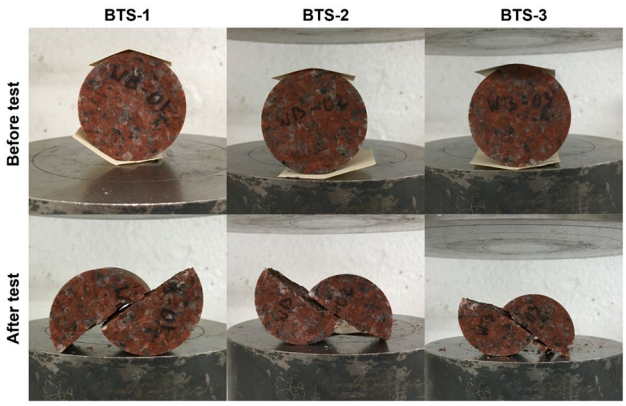

Fig. 9 Images of the specimens before and after completion of the tests

by the hydraulic press was converted to indirect tensile strength using the following equation (International Society for Rock Mechanics 1978):

$$\sigma_t = \frac{2P}{\pi Dt}$$

where P is the load at failure, D is the diameter of the specimen, and t is the thickness of the specimen.

Appendix B

The results in Sect. 3.2 correspond to BBMs that have four different grain types and 10 corresponding mineral–mineral associations, with properties listed in Tables 7 and 8, respectively. To ensure that the observed behaviors are not a function of the specific set of micro-properties or material heterogeneity (i.e., mismatch in grain elastic and contact properties) and more generally depict the role of geometric heterogeneity, additional models were run with different micro-properties.

(1) Effect of contact tensile strength

Contact tensile strength directly controls the emergent macroscopic tensile strength of BBMs (Kazerani and Zhao 2010; Fabjan et al. 2015). To understand its influence, two sets of models were run, where the contact tensile strengths were varied by ± 25% (with respect to those listed in Table 8). Each set consisted of 72 models: 6 deterministic (3 specimens, 2 faces each), 6 semi-deterministic (3 specimens, 2 faces each), 30 Voronoi HGS (3 specimens, 2 faces each, 5 realizations per face), and 30 Voronoi UGS (3 specimens, 2 faces each, 5 realizations per face). Model results and overall statistics are presented in Fig. 10 and Table 12, respectively. For ease of comparison, model strengths corresponding to

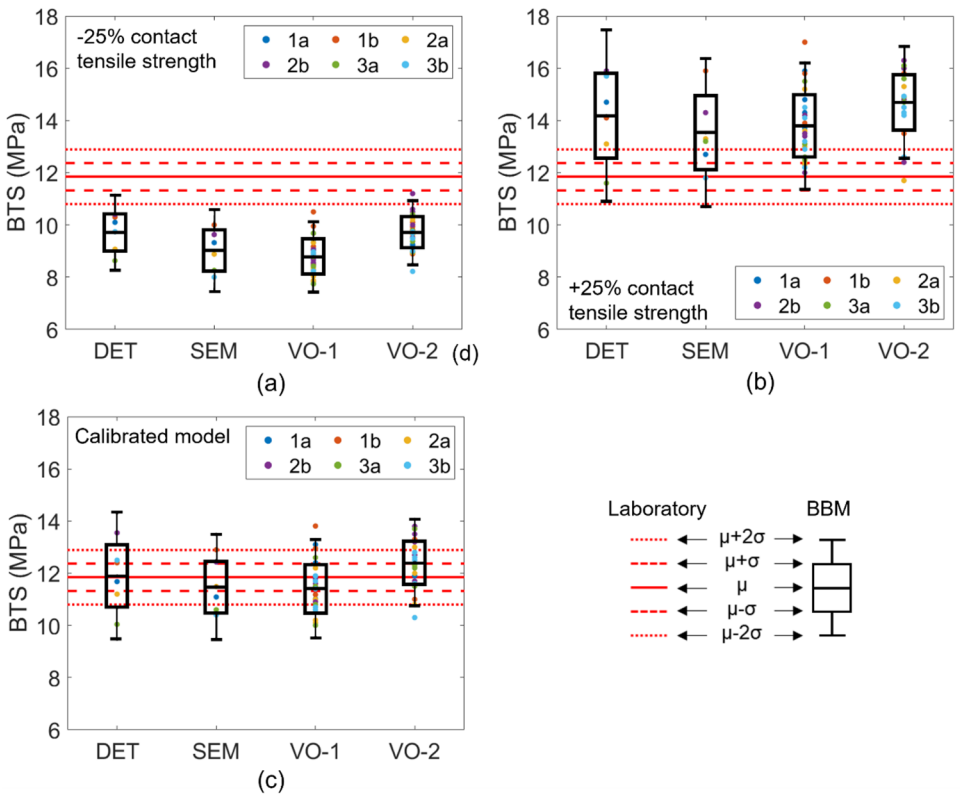

Fig. 10 Comparison of laboratory results (LAB) against corresponding deterministic (DET), semi-deterministic (SEM), Voronoi HGS (VO-1), and Voronoi UGS (VO-2) BTS. **a** Comparison with 25% decrease in contact tensile strength, **b** Comparison with 25% increase in contact tensile strength, and **c** Comparison with no change in contact tensile strength, i.e., calibrated properties

Table 12 Summary of the average BTS generated using each type of model

Case	Deterministic		Semi-deterministic		Voronoi HGS		Voronoi UGS	
	μ (MPa)	σ (MPa)	μ (MPa)	σ (MPa)	μ (MPa)	σ (MPa)	μ (MPa)	σ (MPa)
Calibrated	11.9	1.2	11.5	1.0	11.4	0.9	12.4	0.8
− 25%	9.7	0.7	9.0	0.8	8.8	0.7	9.7	0.6
+ 25%	14.2	1.6	13.5	1.4	13.8	1.2	14.7	1.1

the calibrated set of micro-properties are added to Fig. 10 and Table 12.

As expected, the BTS increased and decreased for all four model types with an increase or decrease in contact tensile strength, respectively. The change in simulated BTS is less than 25% in the majority of the models because of the complex non-linear relationship between contact strength and local fracture development. With respect to the calibrated case, the average mean strengths changed by similar amounts (2–2.7 MPa; Table 12), such that the strengths are similar across the four model types in both the + 25% and − 25% cases. This supports the general observation in Sect. 3.2 that there is a limited effect of geometric heterogeneity on modeled BTS.

The variability in BTS follows the same trend as the change introduced in the contact tensile strength, i.e., standard deviation (STD) of − 25% case < STD calibrated < STD + 25% case. This is explained by the greater absolute heterogeneity in the contact tensile strength in the + 25% case in comparison with the − 25% case. For example, if the tensile strengths of two contact types are 2 MPa and 3 MPa, then the difference between them changes to 0.75 MPa (lower heterogeneity) and 1.25 MPa (higher heterogeneity) with − 25% and + 25% change, respectively. It follows that the − 25% model is more homogeneous in an absolute sense than the + 25% model, and hence demonstrates lower variability in BTS. This also means that contact strength heterogeneity has some influence on BTS, but the influence is similar across the different grain structures considered.

(B) Effect of material heterogeneity

For this analysis, two different types of parameter homogenization were considered (Sinha and Walton 2020).

Grain property homogenization: 6 sets of grain elastic properties were computed for the 6 faces (BTS-1A, BTS-1B, BTS-2A, BTS-2B, BTS-3A, BTS-3B) by weight averaging the properties listed in Table 7 with the mineral proportions in Table 1. All grains in the model were assigned 1 set (out of 6 sets) of elastic property depending on which face it represented. No homogenization of the contact property was performed.

Complete homogenization: In addition to the grain property homogenization, contact properties were also homogenized by weight averaging the properties listed in Table 8 with the associated total contact length in every model. Since the contact lengths for the 10 mineral–mineral associations varied across the models, the weighted average calculation had to be performed individually for each model. Simply stated, in these models, a single set of grain and contact properties was assigned to all the grains and contacts.

Similar to the previous analysis considering variations in tensile strength, 72 models were run for each case—6 deterministic (3 specimens, 2 faces each), 6 semi-deterministic (3 specimens, 2 faces each), 30 Voronoi HGS (3 specimens, 2 faces each, 5 realizations per face), and 30 Voronoi UGS (3 specimens, 2 faces each, 5 realizations per face). Results are presented in Fig. 11 and Table 13. The following observations are made:

- BTS increases with material property homogenization, consistent with the previous analysis. Homogenization reduces the local tensile stresses developing within a BBM (Dey and Wang 1981; Kranz 1983; Sinha and Walton 2020) and thereby delays fracture development and failure.
- With respect to the calibrated case, the average BTS for grain property homogenized models increased by 1.1–1.9 MPa and the variability is similar across all model types (Fig. 11a). It is not clear why the VO-HGS model exhibited ~ 1 MPa lower average strength than the other three types. In any case, the simple VO-UGS model demonstrated similar strength distribution as the deterministic and semi-deterministic models, consistent with the observations in Sect. 3.2.
- For the complete homogenized models (Fig. 11b), the average strengths are similar across the four model types. It is noted here that 5 realizations were run per face for both VO-HGS and VO-UGS models, but no/minimal deviation was observed (as a result, there is no scatter; see Fig. 11b). This is because the grain structure in the 5 realizations for a face was the same (refer to Sect. 2.2 and Table 6) and homogenizing both the contact and grain properties essentially led to very similar realizations (same grain structure, same grain properties, and very similar contact properties).
- Overall, the average strengths are similar across the four grain structures considered, meaning that the simplest UGS model can be used instead of the more complex

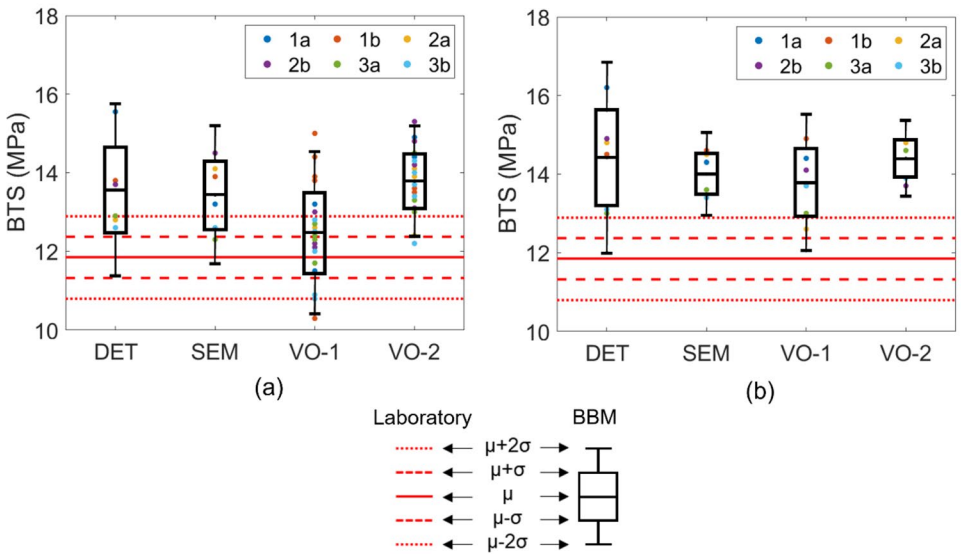

Fig. 11 Comparison of laboratory results (LAB) against corresponding deterministic (DET), semi-deterministic (SEM), Voronoi HGS (VO-1), and Voronoi UGS (VO-2) BTS. **a** Comparison with grain property homogenization, **b** Comparison with grain and contact property homogenization

Table 13 Summary of the average BTS generated using each type of model

Case	Deterministic		Semi-deterministic		Voronoi HGS		Voronoi UGS	
	μ (MPa)	σ (MPa)	μ (MPa)	σ (MPa)	μ (MPa)	σ (MPa)	μ (MPa)	σ (MPa)
Calibrated	11.9	1.2	11.5	1.0	11.4	0.9	12.4	0.8
Grain homogenization	13.5	1.1	13.4	0.9	12.5	1.0	13.8	0.7
Complete homogenization	14.4	1.2	14	0.5	13.8	0.9	14.4	0.5

deterministic or semi-deterministic model for practical purposes, whether homogeneous or heterogeneous micro-properties are used. The similar performance obtained using the different grain structure assumptions suggests that the conclusions of this study regarding the validity of the Voronoi approach could perhaps be extended to the simulation of monomineralic rocks.

Acknowledgements The authors would like to extend their gratitude for the financial support. Special thanks to Dr. Katharina Pfaff of the automated mineralogy laboratory, Jae Erickson of the thin-section laboratory, and Bruce Yoshioka, Brent Duncan, Omid Frough, and Muthu Vinayak of the Earth Mechanics Institute at the Colorado School of Mines for their help during the laboratory tests and analyses.

Author Contributions CECI: conceptualization, methodology, software, validation, formal analysis, investigation, data curation, writing—original draft, writing—review and editing, visualization. SS: methodology, software, validation, formal analysis, investigation, data curation, writing—original draft, writing—review and editing, visualization. GW: conceptualization, methodology, resources, writing—review and editing, supervision, project administration, funding acquisition. EH: conceptualization, methodology, resources, writing—review and editing.

Funding This work was supported by the National Institute for Occupational Safety and Health (NIOSH) under Grant Number 200-2016-90154.

Data Availability The data that support the findings of this study are available from the corresponding author upon reasonable request.

Declarations

Conflict of Interest The authors declare that they have no known competing financial interests or personal relationships that could have appeared to influence the work reported in this paper.

References

Abdelaziz A, Zhao Q, Grasselli G (2018) Grain based modelling of rocks using the combined finite-discrete element method. Comput Geotech 103:73–81. https://doi.org/10.1016/j.compgeo.2018.07.003

ASTM International (2001) ASTM D 3967–95a (reapproved 2001): standard test method for splitting tensile strength of intact rock core specimens. In Annual Book of ASTM Standards: Vol. 04.08. West Conshohocken, PA: ASTM International

Autodesk Inc., (2019) AutoCAD 2020 Product Help. https://knowledge.autodesk.com/support/autocad/downloads/caas/downloads/content/download-install-autocad-2020-product-help.html. Accessed 17 July 2022

Azocar K (2016) Investigating the mesh dependency and upscaling of 3D grain-based models for the simulation of brittle fracture processes in low-porosity crystalline rock. Queen's University, Kingston

Bahrani N, Kaiser PK, Valley B (2014) Distinct element method simulation of an analogue for a highly interlocked, non-persistently jointed rockmass. Int J Rock Mech Min Sci 71:117–130. https://doi.org/10.1016/j.ijrmms.2014.07.005

Bewick RP, Kaiser PK, Bawden WF, Bahrani N (2014) DEM simulation of direct shear: 1. rupture under constant normal stress boundary conditions. Rock Mech Rock Eng 47:1647–1671. https://doi.org/10.1007/s00603-013-0490-8

Bobet A, Fakhimi A, Johnson S, Morris J, Tonon F, Yeung MR (2009) Numerical models in discontinuous media: review of advances for rock mechanics applications. J Geotech Geoenviron Eng 135(11):1547–1561

Cai JG, Zhao J (2000) Effects of multiple parallel fractures on apparent attenuation of stress waves in rock masses. Int J Rock Mech Min Sci 37:661–682. https://doi.org/10.1016/S1365-1609(00)00013-7

Chen W, Konietzky H (2014) Simulation of heterogeneity, creep, damage and lifetime for loaded brittle rocks. Tectonophysics 633:164–175. https://doi.org/10.1016/j.tecto.2014.06.033

Chen SG, Cai JG, Zhao J, Zhou YX (2000) Discrete element modelling of an underground explosion in a jointed rock mass. Geotech Geol Eng 18:59–78. https://doi.org/10.1023/A:1008953221657

Chen S, Yue ZQ, Tham LG (2004) Digital image-based numerical modeling method for prediction of inhomogeneous rock failure. Int J Rock Mech Min Sci 41:939–957. https://doi.org/10.1016/j.ijrmms.2004.03.002

Chen W, Konietzky H, Tan X, Frühwirt T (2016) Pre-failure damage analysis for brittle rocks under triaxial compression. Comput Geotech 74:45–55. https://doi.org/10.1016/j.compgeo.2015.11.018

Cho NA, Martin CD, Sego DC (2007) A clumped particle model for rock. Int J Rock Mech Min Sci 44(7):997–1010. https://doi.org/10.1016/j.ijrmms.2007.02.002

Contreras Inga CE, Walton G, Holley E (2021) Statistical assessment of the effects of grain structure representation and micro-properties on the behavior of bonded block models for brittle rock damage prediction. Sustainability 13:7889. https://doi.org/10.3390/su13147889

Cowie S, Walton G (2018) The effect of mineralogical parameters on the mechanical properties of granitic rocks. Eng Geol 240:204–225. https://doi.org/10.1016/j.enggeo.2018.04.021

Cundall PA (1971) A computer model for simulating progressive large-scale movements in blocky rock systems. Proceedings of Int. Society for Rock Mechanics Symposium: Rock Fracture, 129–136

Cundall PA, Strack ODL (1979) A discrete numerical model for granular assemblies. Geotechnique 29(1):47–65. https://doi.org/10.1680/geot.1979.29.1.47

Cunha AP (1990) Scale effects in rock mass. Proceeding of International Workshop on Scale Effects in Rock Masses, Balkema

Dan DQ, Konietzky H (2014) Numerical simulations and interpretations of Brazilian tensile tests on transversely isotropic rocks. Int J Rock Mech Min Sci 71:53–63

Dey TN, Wang CY (1981) Some mechanisms of microcrack growth and interaction in compressive rock failure. Int J Rock Mech Mining Sci Geomech Abstr 18(3):199–209

Diederichs MS (1999) Instability of hard rock masses: The role of tensile damage and relaxation. Ph.D. Thesis, University of Waterloo, Waterloo

Diederichs MS (2003) Rock fracture and collapse under low confinement conditions. Rock Mech Rock Eng 36:339–381. https://doi.org/10.1007/s00603-003-0015-y

Ding X, Zhang L (2014) A new contact model to improve the simulated ratio of unconfined compressive strength to tensile strength in bonded particle models. Int J Rock Mech Min Sci 69:111–119. https://doi.org/10.1016/j.ijrmms.2014.03.008

Eberhardt E (1998) Brittle rock fracture and progressive damage in uniaxial compression, PhD Thesis. ed, Ph.D. Thesis, University of Saskatchewan, Saskatoon, Saskatchewan, Canada. University of Saskatchewan, Saskatoon, Saskatchewan. https://doi.org/10.16953/deusbed.74839

Eberhardt E, Stimpson B, Stead D (1999) Effects of grain size on the initiation and propagation thresholds of stress-induced brittle fractures. Rock Mech Rock Eng 32:81–99. https://doi.org/10.1007/s006030050026

Fabjan T, Ivars DM, Vukadin V (2015) Numerical simulation of intact rock behaviour via the continuum and Voronoi tessellation models: a sensitivity analysis. Acta Geotechnica Slovenica 12:5–23

Farahmand K, Diederichs MS (2015) A calibrated synthetic rock mass (SRM) model for simulating crack growth in granitic rock considering grain scale heterogeneity of polycrystalline rock, in: 49th US Rock Mechanics/Geomechanics Symposium. American Rock Mechanics Association, San Francisco, California

Fredrich JT, Evans B, Wong T-F (1990) Effect of grain size on brittle and semibrittle strength: implications for micromechanical modelling of failure in compression. J Geophys Res. https://doi.org/10.1029/jb095ib07p10907

Gao FQ, Stead D (2014) The application of a modified Voronoi logic to brittle fracture modelling at the laboratory and field scale. Int J Rock Mech Min Sci 68:1–14. https://doi.org/10.1016/j.ijrmms.2014.02.003

Gao F, Stead D, Elmo D (2016) Numerical simulation of microstructure of brittle rock using a grain-breakable distinct element grain-based model. Comput Geotech 78:203–217. https://doi.org/10.1016/j.compgeo.2016.05.019

Garza-Cruz T, Pierce M, Kaiser P (2014) Use of 3DEC to study spalling and deformation associated with tunnelling at depth. Proceedings of the Seventh International Conference on Deep and High Stress Mining 421–434. https://doi.org/10.36487/acg_rep/1410_28_garza-cruz

Ghazvinian E, Diederichs MS, Quey R (2014) 3D random Voronoi grain-based models for simulation of brittle rock damage and fabric-guided micro-fracturing. J Rock Mech Geotech Eng 6:506–521. https://doi.org/10.1016/j.jrmge.2014.09.001

Gui YL, Zhao ZY, Ji J, Wang XM, Zhou KP, Ma SQ (2016) The grain effect of intact rock modelling using discrete element method with voronoi grains. Geotech Lett 6:136–143. https://doi.org/10.1680/jgele.16.00005

Güneş Yilmaz N, Mete Goktan R, Kibici Y (2011) Relations between some quantitative petrographic characteristics and mechanical strength properties of granitic building stones. Int J Rock Mech Min Sci 48:506–513. https://doi.org/10.1016/j.ijrmms.2010.09.003

Insana A, Marla M, Elmo D (2016) Multiscale numerical modelling related to hydrofracking for deep geothermal energy exploration. Proc Eng 158:314–319

International Society for Rock Mechanics (1978) Suggested methods for determining tensile strength of rock materials. Int J Rock Mech Min Sci 15:99–103. https://doi.org/10.1016/0148-9062(78)91494-8

Itasca Consulting Group Inc. (2014) UDEC version 6.0: Universal disctinct element code, user's guide, 4th edn. Itasca Consulting Group Inc., Minneapolis

Jing L (2003) A review of techniques, advances and outstanding issues in numerical modelling for rock mechanics and rock engineering. Int J Rock Mech Min Sci 40:283–353. https://doi.org/10.1016/S1365-1609(03)00013-3

Jing L, Hudson JA (2002) Numerical methods in rock mechanics. Int J Rock Mech Min Sci 39:409–427. https://doi.org/10.1016/S1365-1609(02)00065-5

Jing L, Stephansson O (2007) Fundamentals of discrete element methods for rock engineering—theory and applications. Developments in geotechnical engineering. Elsevier, Amsterdam, pp 365–398

Kazerani T, Zhao J (2010) Micromechanical parameters in bonded particle method for modeling of brittle material failure. Int J Numer Anal Meth Geomech 34:1877–1895. https://doi.org/10.1002/nag.884

Kazerani T, Yang ZY, Zhao J (2012) A discrete element model for predicting shear strength and degradation of rock joint by using compressive and tensile test data. Rock Mech Rock Eng 45:695–709. https://doi.org/10.1007/s00603-011-0153-6

Keikha T, Keykha HA (2013) Correlation between mineralogical characteristics and engineering properties of granitic rocks. Electron J Geotech Eng 18:4055–4065

Kranz RL (1983) Microcracks in rocks: a review. Tectonophysics 100(1–3):449–480

LaBerge GL, Myers PE (1983) Precambrian geology of Marathon county, Wisconsin. Wis Geol Nat Hist Surv Inf Circ 45:88

Lan H, Martin CD, Hu B (2010) Effect of heterogeneity of brittle rock on micromechanical extensile behavior during compression loading. J Geophys Res. https://doi.org/10.1029/2009jb006496

Langford JC, Diederichs MS (2015) Quantifying uncertainty in Hoek-Brown intact strength envelopes. Int J Rock Mech Min Sci 74:91–102. https://doi.org/10.1016/j.ijrmms.2014.12.008

Li D, Wong LN (2013) The Brazilian disc test for rock mechanics applications: review and new insights. Rock Mech Rock Eng 46(2):269–287

Li XF, Li HB, Zhao J (2017a) 3D polycrystalline discrete element method (3PDEM) for simulation of crack initiation and propagation in granular rock. Comput Geotech 90:96–112. https://doi.org/10.1016/j.compgeo.2017.05.023

Li J, Konietzky H, Frühwirt T (2017b) Voronoi-based DEM simulation approach for sandstone considering grain structure and pore size. Rock Mech Rock Eng 50(10):2749–2761

Li XF, Li HB, Zhao J (2019) The role of transgranular capability in grain-based modelling of crystalline rocks. Comput Geotech 110:161–183. https://doi.org/10.1016/j.compgeo.2019.02.018

Li H, Ma H, Shi X, Zhou J, Zhang H, Daemen JJK (2020) A 3D grain-based model for simulating the micromechanical behavior of salt rock. Rock Mech Rock Eng 53:2819–2837. https://doi.org/10.1007/s00603-020-02085-4

Li XF, Li HB, Zhao J (2021a) Transgranular fracturing of crystalline rocks and its influence on rock strengths: insights from a grain-scale continuum–discontinuum approach. Computer Methods Appl Mech Eng. https://doi.org/10.1016/j.cma.2020.113462

Li D, Li B, Han Z, Zhu Q, Liu M (2021b) Evaluation of bi-modular behavior of rocks subjected to uniaxial compression and Brazilian tensile testing. Rock Mech Rock Eng 54(8):3961–3975. https://doi.org/10.1007/s00603-021-02469-0

Lisjak A, Grasselli G (2014) A review of discrete modeling techniques for fracturing processes in discontinuous rock masses. J Rock Mech Geotech Eng 6:301–314. https://doi.org/10.1016/j.jrmge.2013.12.007

Liu G, Cai M, Huang M (2018) Mechanical properties of brittle rock governed by micro-geometric heterogeneity. Comput Geotech 104:358–372. https://doi.org/10.1016/j.compgeo.2017.11.013

Mahabadi OK (2012) Investigating the influence of micro-scale heterogeneity and microstructure on the failure and mechanical behaviour of geomaterials. University of Toronto, Toronto. https://doi.org/10.13140/2.1.2218.9762

Mahabadi OK, Tatone BS, Grasselli G (2014) Influence of microscale heterogeneity and microstructure on the tensile behavior of crystalline rocks. J Geophys Res 119(7):5324–5341. https://doi.org/10.1002/2014JB011064

Martin CD (1993) The strength of massive Lac du Bonnet granite around underground openings. University of Manitoba, Winnipeg

Mayer JM, Stead D (2017) Exploration into the causes of uncertainty in UDEC grain boundary models. Comput Geotech 82:110–123. https://doi.org/10.1016/j.compgeo.2016.10.003

Munjiza A (2004) The combined finite-discrete element method. John Wiley & Sons, Chichester

Nicksiar M, Martin CD (2014) Factors affecting crack initiation in low porosity crystalline rocks. Rock Mech Rock Eng 47:1165–1181. https://doi.org/10.1007/s00603-013-0451-2

Olsson WA (1974) Grain size dependence of yield stress in marble. J Geophys Res 79:4859–4862. https://doi.org/10.1029/jb079i032p04859

Papoulis A, Pillai SU (2002) Probability, random variables, and stochastic processes. Tata McGraw-Hill Education, New York

Park JW, Park C, Song JW, Park ES, Song JJ (2017) Polygonal grain-based distinct element modeling for mechanical behavior of brittle rock. Int J Numer Anal Meth Geomech 41(6):880–898

Peng J, Wong LNY, Teh CI (2017a) Effects of grain size-to-particle size ratio on micro-cracking behavior using a bonded-particle grain-based model. Int J Rock Mech Min Sci 100:207–217. https://doi.org/10.1016/j.ijrmms.2017.10.004

Peng J, Wong LNY, Teh CI (2017b) Influence of grain size heterogeneity on strength and microcracking behavior of crystalline rocks. J Geophys Res 122:1054–1073. https://doi.org/10.1002/2016JB013469

Peng J, Yuen Wong LN, Teh CI (2021) Influence of grain size on strength of polymineralic crystalline rock: new insights from DEM grain-based modeling. J Rock Mech Geotech Eng. https://doi.org/10.1016/j.jrmge.2021.01.011

Perras MA, Diederichs MS (2014) A review of the tensile strength of rock: concepts and testing. Geotech Geol Eng 32(2):525–546. https://doi.org/10.1007/s10706-014-9732-0

Potyondy DO, Cundall PA (2004) A bonded-particle model for rock. Int J Rock Mech Min Sci 41:1329–1364. https://doi.org/10.1016/j.ijrmms.2004.09.011

Potyondy DO (2012) A flat-jointed bonded-particle material for hard rock. Proceedings of the 46th US Rock Mechanics/Geomechanics Symposium, Chicago, Illinois, Paper No. 501

Přikryl R (2001) Some microstructural aspects of strength variation in rocks. Int J Rock Mech Min Sci 38:671–682. https://doi.org/10.1016/S1365-1609(01)00031-4

Quey R (2019) Neper reference manual: the documentation for Neper 3.5.1. Romain Quey

Quey R, Renversade L (2018) Optimal polyhedral description of 3D polycrystals: method and application to statistical and synchrotron X-ray diffraction data. Comput Methods Appl Mech Eng 330:308–333. https://doi.org/10.1016/j.cma.2017.10.029

Quey R, Dawson PR, Barbe F (2011) Large-scale 3D random polycrystals for the finite element method: generation, meshing and remeshing. Comput Methods Appl Mech Eng 200:1729–1745. https://doi.org/10.1016/j.cma.2011.01.002

Sajid M, Coggan J, Arif M, Andersen J, Rollinson G (2016) Petrographic features as an effective indicator for the variation in strength of granites. Eng Geol 202:44–54. https://doi.org/10.1016/j.enggeo.2016.01.001

Scholtès L, Donzé FV (2013) A DEM model for soft and hard rocks: role of grain interlocking on strength. J Mech Phys Solids 61(2):352–369. https://doi.org/10.1016/j.jmps.2012.10.005

Shea WT, Kronenberg AK (1993) Strength and anisotropy of foliated rocks with varied mica contents. J Struct Geol 15:1097–1121. https://doi.org/10.1016/0191-8141(93)90158-7

Sheskin DJ (2003) Handbook of parametric and nonparametric statistical procedures. Chapman and Hall/CRC, Boca Raton

Sims PK, Schulz KJ, Dewitt E, Brasaemle B (1993) Petrography and geochemistry of early Proterozoic granitoid rocks in Wisconsin

magmatic terranes of Penokean Orogen, Northern Wisconsin. US Geological Survey, Bulletin 1904-J, p 31. https://doi.org/10.3133/b1904J

Singh SK (1988) Relationship among fatigue strength, mean grain size and compressive strength of a rock. Rock Mech Rock Eng 21:271–276. https://doi.org/10.1007/BF01020280

Sinha S (2020) Advancing continuum and discontinuum models of brittle rock damage and rock-support interaction. Ph.D. Thesis, Colorado School of Mines, Golden, Colorado, USA

Sinha S, Walton G, (2018) Application of micromechanical modeling to prediction of in-situ rock behavior. In: 52nd US Rock Mechanics/Geomechanics Symposium. American Rock Mechanics Association, Seattle, Washington

Sinha S, Walton G (2020) A study on Bonded Block Model (BBM) complexity for simulation of laboratory-scale stress-strain behavior in granitic rocks. Computers Geotech 118:103363. https://doi.org/10.1016/j.compgeo.2019.103363

Sinha S, Shirole D, Walton G (2020) Investigation of the micromechanical damage process in a granitic rock using an inelastic bonded block model (BBM). J Geophys Res 125(3):e2019JB018844. https://doi.org/10.1029/2019JB018844

Sinha S, Abousleiman R, Walton G (2022) Effect of damping mode in laboratory and field-scale Universal Distinct Element Code (UDEC) models. Rock Mech Rock Eng 55(5):2899–2915

Sprunt ES, Brace WF (1974) Direct observation of microcavities in crystalline rocks. Int J Rock Mech Mining Sci Geomech Abstr 11(4):139–150

Staub I, Andersson JC, Magnor B (2004) Äspö pillar stability experiment: geology and mechanical properties of the rock in TASQ. Svensk Kar. ed., Stockholm

Tan X, Konietzky H, Chen W (2016) Numerical simulation of heterogeneous rock using discrete element model based on digital image processing. Rock Mech Rock Eng 49(12):4957–4964

Tapponnier P, Brace WF (1976) Development of stress-induced microcracks in Westerly granite. Int J Rock Mech Mining Sci Geomech Abstr 13(4):103–112

Tuğrul A, Zarif IH (1999) Correlation of mineralogical and textural characteristics with engineering properties of selected granitic rocks from Turkey. Eng Geol 51:303–317. https://doi.org/10.1016/S0013-7952(98)00071-4

Villeneuve MC, Diederichs MS, Kaiser PK (2012) Effects of grain scale heterogeneity on rock strength and the chipping process. Int J Geomech 12(6):632–647

Wadell H (1933) Sphericity and roundness of rock particles. J Geol 41:310–331. https://doi.org/10.1086/624040

Wang X, Cai M (2018) Modeling of brittle rock failure considering inter- and intra-grain contact failures. Comput Geotech 101:224–244. https://doi.org/10.1016/j.compgeo.2018.04.016

Wang X, Cai M (2019) A comprehensive parametric study of grain-based models for rock failure process simulation. Int J Rock Mech Min Sci 115:60–76. https://doi.org/10.1016/j.ijrmms.2019.01.008

West I, Walton G, Sinha S, (2020) Simulating the Behavior of Compressively Loaded Blanco Mera Granite Using Bonded Block Models. Proceedings of the 54th US Rock Mechanics/Geomechanics Symposium, Paper No. 1209

Wong RHC, Chau KT, Wang P (1996) Microcracking and grain size effect in Yuen Long marbles. Int J Rock Mech Mining Sci Geomech 33:479–485. https://doi.org/10.1016/0148-9062(96)00007-1

Xu T, Fu TF, Heap MJ, Meredith PG, Mitchell TM, Baud P (2020) Mesoscopic damage and fracturing of heterogeneous brittle rocks based on three-dimensional polycrystalline discrete element method. Rock Mech Rock Eng. https://doi.org/10.1007/s00603-020-02223-y

Yesiloglu-Gultekin N, Sezer EA, Gokceoglu C, Bayhan H (2013) An application of adaptive neuro fuzzy inference system for estimating the uniaxial compressive strength of certain granitic rocks from their mineral contents. Expert Syst Appl 40:921–928. https://doi.org/10.1016/j.eswa.2012.05.048

Yu Y, Yin J, Zhong Z (2006) Shape effects in the Brazilian tensile strength test and a 3D FEM correction. Int J Rock Mech Min Sci 43(4):623–627

Zhang Y, Wong LNY (2018) A review of numerical techniques approaching microstructures of crystalline rocks. Comput Geosci 115:167–187. https://doi.org/10.1016/j.cageo.2018.03.012

Zhou J, Lan H, Zhang L, Yang D, Song J, Wang S (2019) Novel grain-based model for simulation of brittle failure of Alxa porphyritic granite. Eng Geol 251:100–114. https://doi.org/10.1016/j.enggeo.2019.02.005

Zhu D-F, Tu S-H, Ma H, Zhang X (2017) A 3D Voronoi and subdivision model for calibration of rock properties. Modell Simul Mater Sci Eng 25:25